Gravitational and other shifts of neutron, hydrogen, antihydrogen, muonium, and positronium whispering gallery and gravitational state interference patterns

V.V. Nesvizhevsky[1],* J.A. Pioquinto[1,2], K. Schreiner[1,3,4,5],
S. Baeßler[2,6], P. Crivelli[7], and E. Widmann[4]

[1] *Nuclear and Particle Physics, Institut Max von Laue - Paul Langevin, Grenoble, France*

[2] *University of Virginia, Charlottesville, Virginia, USA*

[3] *Laboratoire Kastler Brossel, Sorbonne Universite, CNRS, ENS-Universite PSL, College de France, Paris, France*

[4] *Marietta Blau Institut, Austrian Academy of Sciences, Vienna, Austria*

[5] *Vienna Doctoral School in Physics, Vienna, Austria*

[6] *Oak Ridge National Laboratory, Oak Ridge, Tennessee, USA and*

[7] *Institute for Particle Physics and Astrophysics, ETH Zurich, Zurich, 8093, Switzerland*

(Dated: October 14, 2025)

Abstract

Recently, a shift of a neutron whispering-gallery interference pattern due to an external magnetic field gradient was measured. By analogy, a similar phenomenon can be observed with other particles and forces. In particular, a gravitational shift of the neutron whispering gallery can be easily observed with cold or very cold or ultracold neutrons, and the developed methods can be used for observing/searching for other shifts in fundamental neutron physics experiments, for instance, for measuring the gravitational constant or constraining the neutron electric charge. A peculiar feature of analogous atomic (anti-atomic) experiments is the much smaller effective critical energies of the materials of atomic (anti-atomic) mirrors. We evaluated parameters that make a measurement of the hydrogen and antihydrogen whispering gallery and their gravitational shifts feasible. A series of such measurements will be made with neutrons at the PF1B/PF2/D17 facilities at the ILL, as well as with hydrogen or/and deuterium atoms by the GRASIAN collaboration in Vienna and Turku. Such a measurement with antihydrogen atoms may be of interest for the GBAR experiment or other experiments at CERN, which study the gravitational properties of antimatter, or the ASACUSA experiment, which is producing a beam of slow $\overline{\mathrm{H}}$ atoms. Quantum reflection of muonium and positronium from material surfaces opens the possibility of observing whispering-galley states, although such measurements remain experimentally challenging. The observation of gravitational shifts is particularly demanding because of the extremely short lifetimes of these systems. Measurements of whispering gallery with all these atoms and particles yield unique information on the quantum reflection properties at surfaces, providing valuable input for both fundamental and surface studies.

I. INTRODUCTION

Whispering gallery is a well-known phenomenon observed in a variety of realizations, including sound waves in the air [1–4] and electromagnetic waves of a broad wavelength range [5–18]. It consists of wave localization in the vicinity of concave mirrors and is expected for waves of various nature.

The Whispering Gallery States (WGS) of massive particles depend on their masses. Previously, WGS were considered for atoms [19, 20] and antiatoms [21] as well as observed for

* Corresponding author: nesvizhevsky@ill.eu

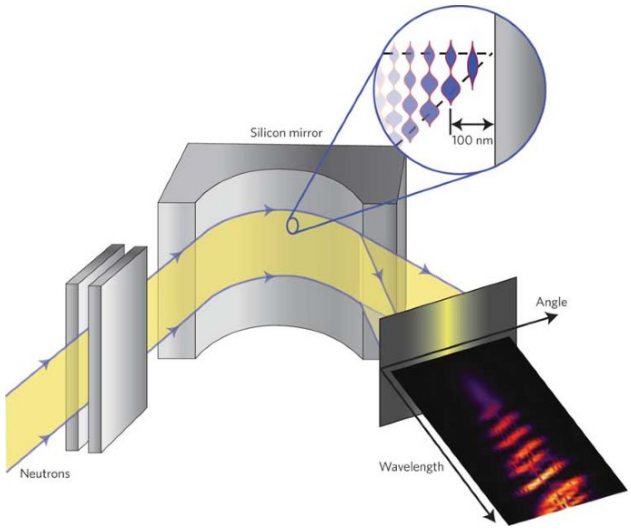

FIG. 1. An angularly collimated white neutron beam arrives to the entrance of a concave cylindrical mirror at a small grazing angle to the cylinder surface. Some neutrons are trapped in WGS and continue following the surface towards the exit of the cylindrical mirror. Due to WGS, an interference pattern is observed when measuring simultaneously longitudinal and tangential components of neutron velocity. Longitudinal component of velocity (neutron wavelength) is measured using the time-of-flight technique. Tangential component of velocity (the angle of escape from the mirror edge) is measured in a position-sensitive detector installed at a certain distance from the exit of the cylindrical mirror (the figure is copied from ref. [27]).

neutrons [22–25] and electrons [26].

The WGS method with neutrons is illustrated in Fig. 1 (copied from ref. [27]).

Within a certain simplification, neutrons with an energy of their tangential motion smaller than the critical energy of the mirror material (the neutron-nuclei optical potential [28] introduced by Enrico Fermi in 1936) are reflected. Neutrons with an energy of their tangential motion larger than that are not reflected, and subsequently lost. After several quasi-classical bounces, this energy filter conserves subbarrier neutrons and efficiently eliminates the above barrier neutrons.

A magnetic shift of the WGS of neutrons has been observed and the sensitivity of such an experiment to a small additional force (of magnetic nature) has been experimentally evaluated [29]. For the small prototype used and its short measurement time, the ratio of magnetic and centrifugal forces was as small as $\sim 10^{-5}$. The sensitivity of the method might

be further increased by many orders of magnitude by properly adjusting the experimental parameters, as explained below.

Due to the approximate equality of the masses of the neutron (n), hydrogen (H) and antihydrogen ($\overline{\mathrm{H}}$) atoms, the same approach can be applied to the analysis of the feasibility of observing the WGS of n, H or $\overline{\mathrm{H}}$, as well as the gravitational shifts of them. A major difference are the relatively small values of characteristic critical energies of mirrors for H and $\overline{\mathrm{H}}$ [30] compared to those for neutrons.

In case of the WGS of H and $\overline{\mathrm{H}}$, the quantum reflection (QR) from the surface would provide one wall for the trapping potential well, while the effective centrifugal acceleration would provide the other wall. QR has been observed and considered for many types of atoms and antiatoms [31–45]. Although QR of $\overline{\mathrm{H}}$ has not been observed, there is no doubt that it exists because it is based on the same quantum mechanical mechanism as QR of H.

Two exotic atoms might also be of interest in this context: muonium (Mu) and positronium (Ps). Due to the small masses of Mu and Ps, and the correspondingly large wavelengths of these atoms, a huge increase in the probability of their QR and the effective critical energy of the mirrors is expected.

Due to the very short lifetime of Mu ($\tau^{Mu} \sim 2.2 \cdot 10^{-6}$ s), a gravitational shift of the WGS of Mu is hard to observe; however, observation of the WGS of Mu might be feasible.

The lifetime of ortho-Ps (the triplet state) in the ground state is too short ($\tau^{Ps} \sim 1.42 \cdot 10^{-7}$ s). However, the lifetimes of the highly excited Ps states (Rydberg states) can be much larger. They are about twice the corresponding radiative lifetimes of hydrogenic states, owing to the reduced mass of Ps being half that of the electron–proton system. An important exception is the metastable 2S state, whose decay is still dominated by the 3γ annihilation channel, with a lifetime scaling as n^3. For this state, the total lifetime amounts to $\tau_{2\mathrm{S}}^{\mathrm{Ps}} \sim 1.136$ μs, whereas the purely radiative lifetime would reach about $\sim 2.44 \cdot 10^{-1}$ s, i.e. twice the value for H.

Quantum experiments can provide high sensitivity and/or precision in the cases where they can be performed. For example, neutrons in Gravitational Quantum States (GQS) between the gravitational field of Earth on top and a flat mirror on bottom are useful for searching for exotic interactions and other phenomena beyond the Standard Model [46–69]. GQS of $\overline{\mathrm{H}}$ are of interest in investigating the gravitational interaction of antimatter; the methods could be based on refs. [70–73]. The characterization of WGS of n, H, $\overline{\mathrm{H}}$, Mu and

Ps can also be turned to explore these and other phenomena, in particular for searches for new short-range interactions [74–78] or violations of the weak equivalence principle, Lorentz invariance and CPT symmetry [79]. WGS or GQS can also be used in the measurement of fundamental constants. Finally, the characterization of QR of atoms and antiatoms is a subject of considerable interest in itself.

In Section II, we present a general method to optimize the WGS parameters of n, H, $\overline{\mathrm{H}}$, Mu, Ps, etc.

In Section III, we propose some applications of the method of neutron WGS shifts, in particular measurements of the gravitational constant G and placing constraints for a neutron electric charge q_{n}. An observation of a gravitational shift of the WGS of neutrons would provide another example in the "zoo" of quantum phenomena in the gravitational field, in addition to COW (Colella-Overhauser-Werner) [80] and gravitational quantum states (GQS) [70].

In Section IV, we describe a possible scheme for measuring the WGS of H. Note that almost "ideal" conditions for observing H WGS are naturally fulfilled in the experiments of the GRASIAN Collaboration [81, 82]. Due to the low critical energies of any mirror for H, observing the gravitational shift seems feasible. In addition, such experiments with H provide almost one-to-one prototyping of possible future experiments with $\overline{\mathrm{H}}$.

In Section V, we describe a possible scheme for measuring the WGS of $\overline{\mathrm{H}}$. Here, the peculiarity of the choice of experimental parameters is to cope with the large velocity of $\overline{\mathrm{H}}$, because cooling the $\overline{\mathrm{H}}$ is a rather difficult task. Such a scheme might be of interest for GBAR, or other $\overline{\mathrm{H}}$ experiments at CERN, in view of the major efforts to directly measure the gravitational interaction of antimatter [83–88]. The ASACUSA collaboration has recently succeeded in producing an $\overline{\mathrm{H}}$ beam of velocity similar to the existing H beams, albeit with still lower phase space density [89]. If the latter can be improved, WGS measurements with $\overline{\mathrm{H}}$ will become possible in a way similar to H.

In Section VII, we describe the WGS of Mu. In this case, we optimize the experiment to the parameters of the existing Mu source [90].

In Section VIII, we describe the WGS of Ps. Particular attention is paid to the possibility of observing a gravitational shift of the WGS of Ps.

II. A METHOD TO EVALUATE PARAMETERS OF NEUTRON, HYDROGEN, ANTIHYDROGEN, MUONIUM, POSITRONIUM AND OTHER WGS

GQS have proven to be able to provide high sensitivity and/or precision experiments. However, the use of GQS spectrometric and interferometric methods requires sufficiently long observation times of the particles in GQS, which is not always easy to realize in practice because of the high particle velocities or short particle lifetimes.

A. Characteristic parameters of the GQS of neutron, hydrogen, and antihydrogen

Thus, for the particle mass of ~ 1 atomic units (n, H and $\overline{\mathrm{H}}$), the characteristic parameters of GQS (the acceleration a_{GQS}, the energy of GQS in the ground state $E_{GQS}^{(n,H,\bar{H})}$, the size (height) $l_{GQS}^{(n,H,\bar{H})}$ and the formation time of GQS $\tau_{GQS}^{(n,H,\bar{H})}$ are the following:

$$a_{GQS} = g \sim 9.8 \text{ m/s}^2 \quad , \tag{1a}$$

$$E_{GQS}^{(n,H,\bar{H})} = \sqrt[3]{\frac{\hbar^2 \cdot m^{(n,H,\bar{H})} \cdot a_{GQS}^2}{2}} \sim 6.0 \cdot 10^{-13} \ eV \quad , \tag{1b}$$

$$l_{GQS}^{(n,H,\bar{H})} = \frac{E_{GQS}^{(n,H,\bar{H})}}{m^{(n,H,\bar{H})} \cdot a_{GQS}} \sim 5.9 \cdot 10^{-6} \text{ m} \quad , \tag{1c}$$

$$\tau_{GQS}^{(n,H,\bar{H})} = \frac{\hbar}{E_{GQS}^{(n,H,\bar{H})}} \sim 1.1 \cdot 10^{-3} \text{ s} \quad . \tag{1d}$$

Let the observation time $t_{GQS}^{(n,H,\bar{H})}$ (the flight time of the particle through the setup, in the flow-through measurement mode) be

$$\beta_{GQS}^{(n,H,\bar{H})} \sim 10 \tag{2}$$

times larger than $\tau_{GQS}^{(n,H,\bar{H})}$ (Eq. 1d), to have the population in the GQS well stabilized:

$$t_{GQS}^{(n,H,\bar{H})} = \beta_{GQS}^{(n,H,\bar{H})} \cdot \tau_{GQS}^{(n,H,\bar{H})} \sim 1.1 \cdot 10^{-2} \text{ s} \quad . \tag{3}$$

The difficulty of making and polishing mirrors increases sharply as the size of the mirror increases. For a mirror length $L_{GQS}^{(n,H,\bar{H})}$ equal to the standard mirror length in neutron GQS experiments:

$$L_{GQS}^{(n,H,\bar{H})} \sim 0.3 \text{ m} \quad , \tag{4}$$

the maximum particle velocity, which meets the condition (3) is then

$$V_{GQS}^{(n,H,\bar{H})} = \frac{L_{GQS}^{(n,H,\bar{H})}}{t_{GQS}^{(n,H,\bar{H})}} \sim 2.7 \cdot 10^{1} \text{ m/s} \quad . \tag{5}$$

Increasing the mirror length $L_{GQS}^{n,H,\bar{H}}$ (Eq. 4) by a small factor does not change our conclusion.

B. A motivation to use WGS

Thus, such experiments are possible with Ultra-Cold Neutrons (UCN) [91] and with a soft fraction of the spectrum of Very Cold Neutrons (VCN). However, this is an insignificant part of the spectrum of thermal neutron (TN) or cold neutron (CN) sources. The same estimate is valid for the H and $\overline{\text{H}}$ atoms. That is, one needs to implement sources of ultra-cold (anti)atoms to increase the fluxes of such particles.

On the other hand, the WGS method allows for the use of faster particles because the energy of WGS $E_{WGS}^{(n,H,\bar{H})}$ could be greater than $E_{GQS}^{(n,H,\bar{H})}$, thus the characteristic time of formation of WGS $\tau_{WGS}^{(n,H,\bar{H})}$ might be shorter than $\tau_{GQS}^{(n,H,\bar{H})}$. Therefore, precision spectroscopic and interferometric methods using WGS can still be used.

In the following sections, we will apply a simple method to optimize experiments with n, H, $\overline{\text{H}}$, Mu, and Ps. Both the characteristic parameters of such experiments and the criteria for their optimization differ greatly, so the analysis itself will be performed separately for each case. When discussing the method, we will omit the icons corresponding to different particles/atoms but will restore them in the corresponding sections.

C. An optimization method for designing WGS experiments

For WGS, the effective centrifugal acceleration a_{WGS} is

$$a_{WGS} = \frac{V_{WGS}^2}{R_{WGS}} \quad , \tag{6}$$

where V_{WGS} is the longitudinal velocity of the particles and R_{WGS} is the mirror radius. By "tuning" the values V_{WGS} and R_{WGS}, we can tune the value of a_{WGS}.

Note that by choosing parameters V_{WGS} and R_{WGS}, we can make the centrifugal acceleration greater, equal, or smaller than g. However, the magnitude of the acceleration is

limited from above by the requirement that the characteristic energy E_{WGS} is well below the effective critical energy of the mirror, and it is limited from below by the time required to form the corresponding quantum state. Therefore, the following analysis will be done separately for different particles.

The characteristic energy E_{WGS} of the WGS is related to the characteristic time τ_{WGS} of its formation by the uncertainty relation:

$$E_{WGS} \sim \frac{\hbar}{\tau_{WGS}} \quad , \tag{7}$$

where $\hbar$ is the reduced Planck constant, and

$$\tau_{WGS} \sim \left(\frac{2 \cdot \hbar}{m \cdot a_{WGS}^2} \right)^{\frac{1}{3}} \quad , \tag{8}$$

where m is the mass of the particle. Here we have taken advantage of the fact that the energy differences of low-lying quantum states are similar.

The characteristic size (height) l_{WGS} of WGS is

$$l_{WGS} \sim \left(\frac{\hbar^2}{2 \cdot a_{WGS} \cdot m} \right)^{\frac{1}{3}} \quad . \tag{9}$$

E_{WGS} is limited from above by the value of effective critical energy of the mirror material E_{lim}. Strictly speaking, the concept of critical energy does not apply to the process of quantum reflection (QR) of atoms and antiatoms. We will define it in the following and use it at the initial stage to explain the choice of parameters for this problem. However, for the calculations of interference patterns, we will use a precise calculation of the QR probability for each case studied.

In order to observe an interference pattern, one has to populate at least two quantum states. The exact calculation of the spectrum shaping efficiency is a complex task, which depends on the method of shaping the spectrum and the parameters of the problem. In the case of shaping a neutron spectrum in WGS, this problem is analyzed in detail in ref. [92]. For an approximate assessment, the following rule can be used here and in all similar cases below. Assume

$$\gamma_{WGS} \cdot E_{WGS} \sim E_{lim} \quad . \tag{10}$$

The ground quantum state has a sufficiently long lifetime if $\gamma_{WGS} \sim 3$. Adding excited states adds ~ 1 to γ_{WGS} for each excited state (for simplicity, we neglect the decrease in the energy difference between neighbor states with increasing state number).

Note that in the case of the formation of the neutron spectrum in GQS, the spectrum shaping efficiency is analyzed in detail in refs. [93–99] (this analysis can easily be generalized to GQS of atoms since it is not based on the specifics of the interaction of particles with the surface, but only on the geometry of the absorber/scatterer). It can also be generalized to WGS of all particles discussed in this paper. In the following, we will use the same formula (Eq. (10)) and the simple rule for all GQS and WGS.

The QR probability of atoms and antiatoms does not show a sharp threshold behavior. Therefore, the definition of E_{lim} is specific to the problem to be described, in particular the type of (anti-) atoms, the number of quasi-classical bounces and the mirror material. Here, we define it as follows.

Since in some experiments we measure the anti(atoms) surviving to the mirror edge, and in other experiments we measure the anti(atoms) lost, our criterion will be the condition that the fraction of surviving (anti) atoms is 50%:

$$(P_{QR}(E_{lim}))^{\beta_{WGS}} \sim 0.5 \quad . \tag{11}$$

By analogy to GQS (Eq. 2), the number of quasiclassical bounces is:

$$\beta_{WGS} = t_{WGS}/\tau_{WGS} \quad . \tag{12}$$

All that remains to optimize a specific experiment with a specific particle is to select the number of quasi-classical bounces, calculate the effective critical energy for a specific material, and select the energy range. All other parameters are related by simple formulas. After such optimization of the experiment, we perform an accurate calculation of the interference pattern and check whether the spatial, temporal, and energy resolutions are really sufficient to perform the experiment.

D. A general method to estimate the statistical sensitivity

In this paper, we will consider many examples of phenomena and their realizations. The particle fluxes available for them vary by many orders of magnitude. The characteristic parameters of these phenomena also vary by many orders of magnitude. Finally, specific experimental realizations may also vary. Analyzing the statistical accuracy of all these realizations is a labor-intensive task and should be performed in detail later, case by case.

For now, we propose a universal method for assessing the statistical sensitivity of experiments and encourage the reader to perform such an analysis in their own cases. We have conducted such a preliminary analysis and find that all the cases we describe are feasible or might be feasible under certain conditions.

To estimate the number of events that can contribute to the interference pattern, we calculate the corresponding volume of the particle beam's phase space element. The spatial size of the beam is equal to the beam width ΔY (in the direction parallel to the mirror axis) multiplied by the beam height (in the direction perpendicular to the mirror axis). The beam height, in turn, depends on the characteristic size of a quantum state l_{WGS} and the number of quantum states as $(\gamma_{WGS} \cdot l_{WGS})$ (Eqs. 9, 10). The size of the velocity phase space element is usually unlimited in the direction parallel to the beam axis (if the longitudinal velocity is significantly greater than the transverse velocity). In the direction perpendicular to the mirror axis, it is equal to twice the characteristic velocity corresponding to the quantum state energy E_{WGS} multiplied by the square root of the number of quantum states $\sqrt{(\gamma_{WGS} - 2)}$. The total number of particles in the WGS will be on the order of the fraction of the initial beam flux limited by the phase space element $2 \cdot \Delta Y \cdot \gamma_{WGS} \cdot l_{WGS} \cdot \sqrt{2 \cdot E_{WGS} \cdot (\gamma_{WGS} - 2)/m}$ estimated above, over the total observation time. In order to produce an interference pattern, we need to angularly collimate the incoming beam to be at least a few times smaller than $2 \cdot \sqrt{E_{WGS} \cdot (\gamma_{WGS} - 2)/m}/V_{WGS}$. The total number of counted events must be decreased by this factor.

E. Modeling of GQS and WGS interference patterns

To calculate the interference patterns in the following sections, we follow the formalism developed for the calculation of the UCN and $\overline{\mathrm{H}}$ wave functions in the GQS and WGS potentials [21, 22, 44, 92, 94, 95], the essentials of which we will review in this section.

In each experiment, a coherent beam of particles enters a mirror-absorber/scatterer system where the interference pattern is developed. For both GQS and WGS experiments, this consists of a mirror of length L for particles to bounce on, a uniform force field generated by the gravitational or centrifugal acceleration experienced by the particle, and a rough absorber/scatterer of length L_A and height ΔH above the mirror surface. In the proposed experiments, $L_A \leq L$ and the entrance edge of the absorber is placed to coincide with the

entrance edge of the mirror. The wave function of a particle propagating along the mirror surface can be expressed as a superposition of quasi-bound states, which interfere with each other. For long-lived particles that reflect well from the mirror surface, the interference pattern can be observed by measuring the flux of particles flowing out of the mirror system with a position-sensitive detector downstream of the mirror. To observe the interference pattern for short-lived particles that decay or annihilate with the mirror surface, it is more feasible to observe the flux of particles interacting with the mirror surface as they bounce.

To calculate the flux of particles reaching or interacting with the mirror surface, we must calculate the evolution of the wave function ψ of a particle flowing through the setup. To do this, we define the potential for each section of the experiment and solve the Schrödinger equation. For a sufficiently coherent beam, we assume that an incoming particle's wave function can be modeled as a plane wave. In the transverse direction, perpendicular to the mirror surface, the initial wave function is described as

$$\psi_0 \propto e^{ik_\perp x} \quad . \tag{13}$$

Here, x is the altitude of the particle above the mirror and $k_\perp$ is its wave vector perpendicular to the surface. For simplicity, all calculations are performed assuming a zero incidence angle upon the mirror, so $k_\perp = 0$. The longitudinal direction of the wave function is treated classically, so the propagation time experienced by a particle is determined as $t = z/v$ where z is its longitudinal position and v is its velocity.

The region of the system with a mirror and absorber/scatterer can be described with the potential

$$V(x) = mgx + V_{mirror}(x) + V_{absorber}(x) \quad . \tag{14}$$

The first term is the usual gravitational potential with m being the mass of the particle and g the gravitational acceleration of the Earth. For WGS, the gravitational acceleration g should be substituted with the centrifugal acceleration experienced by the particle a_{WGS} from Eq. (6), with R_{WGS} being the radius of curvature of the mirror. The exact form of V_{mirror} and $V_{absorber}$ depends on the particle that flows through the system and $V_{absorber}$ on the properties of its (rough) surface. For neutrons with small velocities perpendicular to the surface, small enough such that the neutron optical potential of the mirror is larger than the energy of the neutron's perpendicular motion, the mirror will behave as an infinite potential step. For atoms, quantum vacuum fluctuations cause interactions between their

dipole moments and the mirror, giving rise to the van der Waals-Casimir/Polder potential. This potential is very sharp near the surface of the mirror. Atoms with sufficiently low energy will be repelled by a steep change in potential with high efficiency, a phenomenon known as QR [30, 44]. For low enough energies, this interaction can be well described with the scattering length approximation. In this approximation, the mirror surface potential behaves as an infinite potential step to the incident atoms. However, it is important to note that the scattering length can have an imaginary part, which physically corresponds to transmission through the van der Waals-Casimir/Polder potential. This plays a key role in the observation of WGS of exotic atoms.

Without the absorber/scatterer, the potential experienced by the particles in each region is a triangular potential well with an infinite potential step at $x = 0$. We can simply model the presence of the absorber/scatterer as another infinite potential step placed at $x = \Delta H$. The rough surface of the absorber/scatterer introduces a new loss mechanism for states propagating through the system which is not accounted for by the step model. We choose to model this effect generically, as was done in [94, 95] to effectively describe the observation of GQS of neutrons. When populating states in the presence of the absorber/scatterer, states that have a classical height $x_n = E_n/mg \geq \Delta H$ are assumed to be unpopulated by the end of the absorber/scatterer region, and states with $x_n < H$ are assumed to pick up imaginary parts Γ_n to their energy levels

$$E_n - i\frac{\Gamma_n}{2} \quad , \tag{15}$$

which determines the lifetime $\tau_n = \hbar/\Gamma_n$ of the state's population. This lifetime can be estimated by

$$\frac{\Gamma_n}{\hbar} = \omega_n P_n \quad , \tag{16}$$

where ω_n is the classical bouncing frequency and P_n is the probability of tunneling into the classically forbidden region where the absorber/scatterer resides. For particles that decay, a decaying exponential term multiplies the entire wave function to account for the lifetime of the particle.

In each region of the mirror, the wave function can be expressed as

$$\psi(x,t) = \sum_i c_i \psi_i(x,t) e^{-\frac{iE_i t}{\hbar} - \frac{\Gamma_i t}{2\hbar}} \quad , \tag{17}$$

where ψ_i are normalized eigenstates of the described potentials and

$$c_i = \int \psi(x, t = 0)\psi_i(x)dx \tag{18}$$

are the amplitudes for each state. Note that ψ_i are generically part of a bi-orthogonal set since ψ_i are eigenstates of non-Hermitian Hamiltonians, [95, 100] so ψ_i in Eq. (18) is not conjugated. This kind of expression is calculated first for the absorber/scatterer region and then for the absorber/scatterer free region, and the sudden approximation is used to connect the two.

To calculate the flux of particles flowing out of the mirror system and into a detector far from the system, the probability current $\vec{j}$ of the wave packet going into free space should be evaluated at the position of the detector. Assuming the outgoing beam travels in the $\hat{z}$ direction, which corresponds the tangent line of the surface at the end of the mirror, and the transverse direction of the packet with interference is in the $\hat{x}$ direction, the quantity to calculate is

$$\vec{j}(x, z) \cdot \hat{z} = \frac{\hbar}{m}\Im\left(\Psi^* \frac{\partial \Psi}{\partial z}\right) \quad , \tag{19}$$

where z is the position of the detector and x is the position on the detector's surface.

In free space, the wave function $\Psi(x, z)$ can be expressed as a superposition of plane waves with the initial wave packet defined by the Fourier transform of the wave packet at the end of the mirror system

$$\tilde{\psi}(k) = \frac{1}{\sqrt{2\pi}} \int \psi(x, t = T)e^{-ikx}dx \quad , \tag{20}$$

for the propagation time $T = L/v$. Then

$$\begin{aligned} \Psi(x, z) &= \frac{1}{\sqrt{2\pi}} \int_{-\infty}^{\infty} \tilde{\psi}(k)e^{ikx+i\sqrt{k_0^2-k^2}z}dk \\ &\approx \frac{1}{\sqrt{2\pi}} \int_{-\infty}^{\infty} \tilde{\psi}(k)e^{i\left(-\frac{k^2}{2k_0}z+kx\right)}e^{ik_0 z}dk \quad , \end{aligned} \tag{21}$$

where k is the wave vector in the $\hat{x}$ direction and $\sqrt{k_0^2 - k^2}$ is the wave vector in the $\hat{z}$ direction, and k_0 is the magnitude of the total wave vector. In the second line, the paraxial approximation is made since $k << k_0$. The relevant scale of k is l_0^{-1}, so $k^2/2k_0$ has a scale z_0^{-1} where $z_0 = 2k_0 l_0^2$. If $z_0 << z$, then the phase of the exponential in Eq. (21) varies rapidly for the relevant k contributing to the wave packet. In the experiments described in the following, $z/z_0 \gtrsim 10^2$ so we can further approximate the wave function by making

the stationary phase approximation. The details of the approximation are described in Appendix A. The resulting wave function is then

$$\Psi(x,z) \approx \sqrt{\frac{k_0}{z}}\tilde{\psi}\left(k_0\frac{x}{z}\right)e^{i\left(k_0 z+\frac{k_0}{z}\frac{x^2}{2}+\frac{\pi}{4}\right)} \quad . \tag{22}$$

We must also calculate $\partial\Psi/\partial z$, which is most easily done with Eq. (21)

$$\begin{aligned}\frac{\partial\Psi}{\partial z}(x,z) \approx & ik_0\frac{1}{\sqrt{2\pi}}\int_{-\infty}^{\infty}\tilde{\psi}(k)\left(1-\frac{k^2}{2k_0^2}\right)e^{i\left(-\frac{k^2}{2k_0}z+kx\right)}e^{ik_0 z}dk \\ \approx & ik_0\frac{1}{\sqrt{2\pi}}\int_{-\infty}^{\infty}\tilde{\psi}(k)e^{i\left(-\frac{k^2}{2k_0}z+kx\right)}e^{ik_0 z}dk \quad ,\end{aligned} \tag{23}$$

since $k << k_0$. Inserting Eqs. (22) and (23) into (19) yields a current through the detector

$$\vec{j}(x,z)\cdot\hat{z} \approx \frac{\hbar k_0}{m}\frac{k_0}{z}\left|\tilde{\psi}\left(k_0\frac{x}{z}\right)\right|^2 \quad . \tag{24}$$

The current in Eq. (24) assumes that the beam incident upon the mirror system has a velocity distribution of $n(v) = 1$. In reality, the form of $n(v)$ is non-trivial and should be considered in our prediction of the signal. By including $n(v)$ as multiplicative factor and recognizing that $\hbar k_0/m = v$, the particle flux F flowing through the detector should be

$$F(x,v) = n(v)v\frac{k_0}{z}\left|\tilde{\psi}\left(k_0\frac{x}{z}\right)\right|^2 \quad , \tag{25}$$

and then Eq. (25) is taken as our signal. For simplicity and generality, $n(v)v = 1$ for our calculations. We also drop the explicit z dependence from the argument of F since the detector is typically at a fixed distance. For the most accurate prediction, the interference patterns should be multiplied by the flux spectra $n(v)v$ of the beams of interest. To consider experimental resolution effects, on x and v for example, Φ should be convolved with the appropriate resolution functions $R_x(x)$ and $R_v(v)$ such that the new expected signal is

$$\mathcal{F}(x,v) = \int\int F(x',v')R_x(x-x')R_v(v-v')dx'dv' \quad . \tag{26}$$

For particles entering a space with a uniform force field, the expected signal is nearly the same as before but now

$$F(x,v) = n(v)v\frac{k_0}{z}\left|\tilde{\psi}\left(k_0\frac{x+\frac{1}{2}at^2}{z}\right)\right|^2 \quad , \tag{27}$$

where the x coordinate is transformed to follow the trajectories of a classical free fall [101] with an acceleration a and free fall time $t = z/v$. Resolution effects can be considered in the same way as before with Eq. (27), but now with F taking the definition from Eq. (27).

For particles that decay or annihilate on the mirror surface, the signal is taken to be proportional to the probability current of the wave function at the mirror surface $x = 0$ and calculated as a function of the longitudinal position z of the particle along the surface. The current entering the mirror surface for the wave function in Eq. (17) is

$$\vec{j}(z) \cdot \hat{x} = \frac{\hbar}{m} \Im \left(\psi^* \frac{\partial \psi}{\partial x} \right) \Bigg|_{x=0} \quad , \tag{28}$$

which corresponds to a particle flux

$$F(z, v) = n(v) \frac{\hbar}{m} \Im \left(\psi^* \frac{\partial \psi}{\partial x} \right) \Bigg|_{x=0} \quad . \tag{29}$$

In calculations of experiments measuring surface current, $n(v) = 1$. An exponential decaying term is included in Eq. (29) for particles with a lifetime τ. The expected signal then becomes

$$F(z, v) = e^{-t/\tau} n(v) \frac{\hbar}{m} \Im \left(\psi^* \frac{\partial \psi}{\partial x} \right) \Bigg|_{x=0} \tag{30}$$

for $t = z/v$.

Due to our crude treatment of the absorber/scatterer as well as the practical difficulties in understanding its precise behavior in a real experiment, only the probability current after the absorber/scatterer region will be reported. Such complications should not affect strongly the results after the absorber/scatterer region because its primary role is as a state selector, and those states that survive are the ones that interact very little with the absorber/scatterer.

III. APPLICATIONS OF THE METHOD OF NEUTRON WGS SHIFTS

In the experiment to measure the magnetic shift of the WGS of neutrons [29], the additional acceleration was a factor of $\sim 10^5$ lower than the centripetal and did not differ much from the gravitational one. Therefore, the sensitivity to the gravitational shift could be sufficiently high even with such a mirror with a very large curvature. However, it is obvious that just as the effect itself can increase by many orders of magnitude by increasing the time the neutron stays in the gravitational field, so the sensitivity can be increased by many orders of magnitude by decreasing the magnitude of the centripetal acceleration. We will focus on possible applications of this new method for other experiments in the field of fundamental neutron physics.

The general idea is as follows: an additional force to be measured/found is applied along the neutron trajectory, that is, before the mirror, and/or in the mirror area, and/or after the mirror (depending on the conditions of the specific experimental implementation). Such an additional force can, for example, be gravitational, or electrostatic in the case of a search for a hypothetical non-zero electric charge of neutron q_{n}. One of the strategies to increase the sensitivity is to increase the observation time (trajectory length). The neutron velocity, as well as the mirror radius and the boundary energy of its material, are related parameters and should be optimized together.

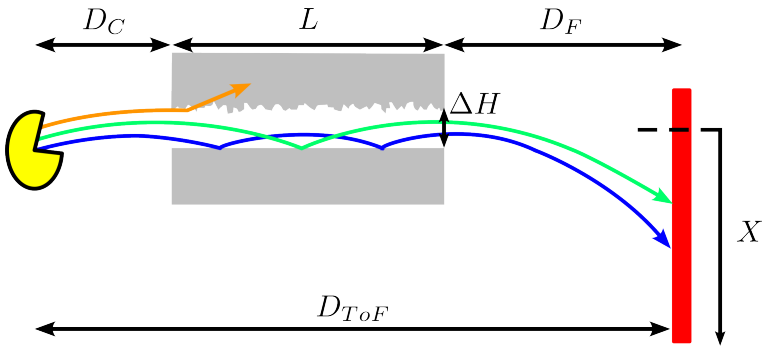

FIG. 2. A schematic of a neutron GQS experiment. A collimated beam of neutrons enters the system through a chopper, placed a distance D_C away from the entrance of the mirror, which enables the measurement of the neutrons' velocity by the time of flight (ToF) method. The beam then enters the mirror absorber/scatterer system. Lower energy GQS can pass through the initial section where an absorber/scatterer of length L is placed a height ΔH above the mirror, while higher GQS are rejected. The lower GQS then propagate along the surface and interfere with each other until reaching the end of the mirror, which has a total length L. The exiting beam enters a free fall region where a time and position sensitive detection system is place a distance D_F from the exit of the mirror. The position of the neutrons on the detector is denoted as X.

A. Sensitivity of a GQS interference pattern measured with very cold neutrons to the gravitational acceleration

This configuration can be implemented using mostly existing equipment and it is not optimized for whatever particular purpose.

The measurement method is equivalent to that used in ref. [24]. Very cold neutrons

(VCN) come from the PF2/VCN instrument at the ILL; it is proposed to use VCN, not UCN, to increase the statistics and simplify the experiment. Time-of-flight measurement is achieved using a chopper in front of the mirrors. The GQS are formed using a 30 cm long horizontal silicon mirror used in refs. [81, 82] and a 30 cm long silicon absorber, the operating principle of which is described in ref. [99]. The interference pattern can be analyzed using a position-sensitive detector installed at a large distance downstream the mirror, or simply by scanning the neutron intensity with a narrow horizontal slit. A scheme of this experiment is shown in Fig. 2, and a simulated interference pattern is shown in Fig. 3. We calculated it for the maximum flight path available at PF2/VCN, $D_{ToF} = 7.3$ m. To resolve the interference pattern, the spatial resolution of the position-sensitive detector should not be worse than ~ 2 mm. Higher spatial resolution also allows for a shorter flight distance, and thus a reduction in intensity losses associated with the angular divergence of the VCN beam in the horizontal plane. The time window of the chopper should not be greater than $\sim$ 1.5 ms. The duty cycle of the chopper can be large, up to $\sim$ 10%, because the temporary overlap of the signals in the detector from neutrons of significantly different velocities is effectively eliminated because they are detected at different heights. Note that here and in the following, the insufficient efficiency of the absorber/scatterer can be taken into account (for approximate calculations) using a simple method. Due to the exponentially strong dependence of the probability of losing a particle in a quantum state on the absorber's height, the definition of height can be renormalized: a significantly lower efficiency corresponds to a small decrease in height.

The calculated sensitivity of such an experiment of 10 days to the value of g is $\sim 10^{-4}$. This is the Cramér-Rao bound for this experiment for $N = 2 \times 10^4$ detected neutrons. The description of this calculation can be found in Appendix B and is calculated with Eq.(B4) where $P(x, v) = \mathcal{F}(x, v)$ corresponds to the Flux simulated using Eqs. (27) and (26). The position resolution function has the shape of a gaussian with two standard deviations corresponding to the stated spatial resolution of the detector. The time resolution is a boxcar function with the width equal to the chopper opening time. More realistic resolution functions should be considered on an experiment by experiment basis.

This experiment can be interpreted as a measurement of the weak equivalence principle (WEP) with a neutron being one of the test masses (and the system that is used to determine the local g as the other). This test of the WEP uses quantum-mechanical properties of the

neutron as the test mass, however, its sensitivity does not come close to the one obtained in Earth-based ($\sim 10^{-13}$ [102]) or satellite-based ($\sim 10^{-15}$ [103]) WEP tests.

Additionally, a measurement of this interference pattern would provide a test for a similar experiment with GQS of H that is being carried out by the GRASIAN collaboration [81, 82]. It would be an intermediate step towards more sensitive experiments described in the following, and it may also provide information on the unexpectedly low GQS population that was observed a few times in previous experiments [94, 104].

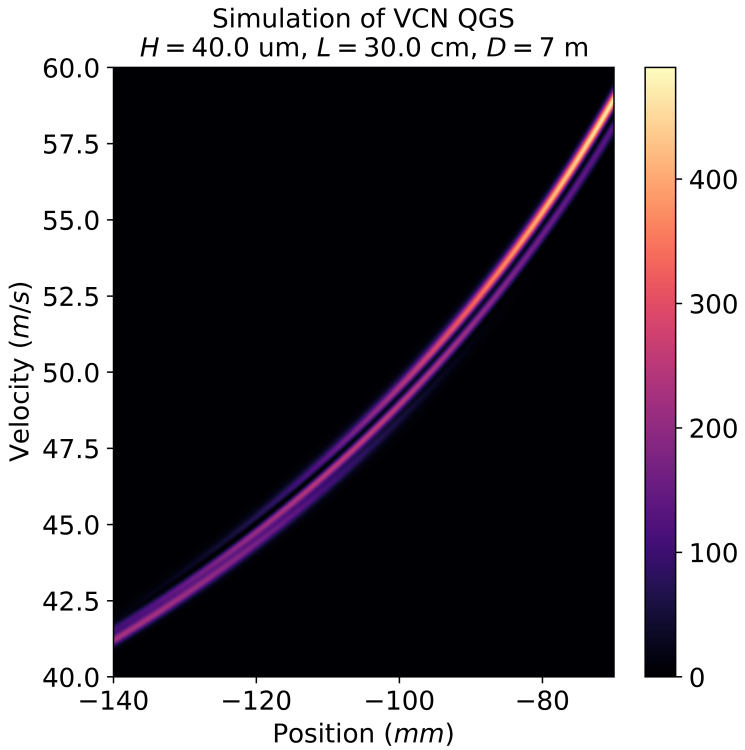

FIG. 3. A simulation of the interference pattern generated by propagating through a mirror-absorber/scatterer system of length $L_{GQS}^{VCN} = 30$ cm. The height of the absorber/scatterer is set to $\Delta H_{GQS}^{VCN} = 40$ μm and the absorber/scatterer is assumed to be very efficient. After exiting the mirror, neutrons enter a free fall region of length $D_{GQS}^{VCN} = 7$ m. The velocities presented in the simulation correspond to the peak in the VCN spectrum at the PF2/VCN instrument.

As the number of GQS (slit height ΔH_{GQS}^{VCN}) increases, the number of interference fringes increases significantly, which means that the sensitivity of the interference pattern increases even more significantly. This improvement is possible with an increase in the spatial resolution of the detector. Note that a thousandfold improvement in spatial resolution has

been demonstrated for several types of neutron detectors [105–109]. However, an even more significant improvement in sensitivity can be obtained using the method presented in the next section.

B. Measurement of the gravitational constant with an UCN WGS interferometer

In order to increase the sensitivity of the method, it seems natural to: a) reduce the longitudinal neutron velocity in order to increase the observation time, b) increase the time neutrons spend in the field, e.g. by providing a longer path length due to multiple specular reflections, and additionally c) reduce the characteristic energy of GQS as the smaller transverse velocity spread allows more specular reflections without overlap of the neutron paths, thus longer observation times.

The decrease in longitudinal velocity is limited by the neutron densities available in the phase space. Thus, in standard experiments with UCN, the characteristic total velocity is ~ 4 m/s, which corresponds to one component of the velocity equal to

$$V_{GQS^{reduced}}^{UCN} \sim 2 \text{ m/s} \quad . \tag{31}$$

Even lower UCN velocities would be an advantage in the future. Given the phase space densities of UCN available worldwide, $\sim 10^3$ UCN/cm^2, the fraction of even slower UCN is insufficient for designing interference experiments. However, provided that much higher UCN densities in phase space are available in the future, say $\sim 10^4$ UCN/cm^3, the optimization parameters of such an interferometer may be revised and the sensitivity greatly improved.

1. Shaping UCN GQS in reduced gravity

Reducing gravitational acceleration can be achieved, for example, by tilting the mirror relative to the Earth's gravitational field. The reduce is limited by the formation time of the GQS. For a small number of quasi-classical bounces,

$$\beta_{GQS^{reduced}}^{UCN} \sim 3 \quad , \tag{32}$$

and a large mirror length,

$$L_{GQS^{reduced}}^{UCN} \sim 1 \text{ m} \quad , \tag{33}$$

the time of formation of GQS in reduced gravity is

$$\tau^{UCN}_{GQS^{reduced}} \sim \frac{L^{UCN}_{GQS^{reduced}}}{\beta^{UCN}_{GQS^{reduced}} \cdot V^{UCN}_{GQS^{reduced}}} \sim 1.7 \cdot 10^{-1} \text{ s} \quad . \tag{34}$$

This value of $\tau^{UCN}_{GQS^{reduced}}$ (Eq. (34)) corresponds to the reduced gravitational acceleration (Eqs. (7,8))

$$g^{UCN}_{reduced} \sim 5.1 \cdot 10^{-3} \text{ m/s}^2 \tag{35}$$

and the angle of inclination of

$$\Delta\Theta \sim 1.8^{'} \quad ; \tag{36}$$

the angle is the inclination of a normal to the mirror relative to the horizontal plane defined by gravity [1].

The characteristic energy of such a quantum state (Eq. (7)) is

$$E^{UCN}_{GQS^{reduced}} \sim 9 \cdot 10^{-15} \text{ eV} \quad . \tag{37}$$

The corresponding (tangential) velocity is

$$(V^{UCN}_{GQS^{reduced}})_{\perp} \sim 10^{-3} \text{ m/s} \quad . \tag{38}$$

The characteristic size of the GQS in reduced gravity is (Eqs. (9,35))

$$l^{UCN}_{GQS^{reduced}} \sim 7.2 \cdot 10^{-5} \text{ m} \quad . \tag{39}$$

The exact calculation of the required slit height between the mirror and the absorber/scatterer, as well as the exact calculation of the absorber/scatterer efficiency, is a complex task, analyzed in detail, for example, in refs. [94–99, 111]. In these same refs., one can find conditions for choosing the parameters of the absorber/scatterer. For an approximate assessment of this value, one can use the same rule as in Eq. (10) and the paragraph below this equation. The size of the slit corresponding to the passage of one quantum state is $\sim 3l^{UCN}_{GQS^{reduced}}$. Adding each next quantum state adds $\sim l^{UCN}_{GQS^{reduced}}$ (Eq. (39)).

[1] Much smaller accelerations of reduced gravity, and therefore much greater sensitivity of the interferometer of the proposed type can in principle be obtained by using not a flow-through but an accumulative mode for shaping the initial quantum state. Here, the experimental challenge consists of the precise installation and control of the mirrors [110]. Therefore, this issue should be better discussed later, provided that the flow-through method for shaping the quantum state is experimentally demonstrated and studied.

The optical system for shaping the GQS in reduced gravity can consist of one or more slits (if the characteristic size of the interference structures on the detector is larger than the size of one slit, or alternatively if the slits are oriented in a way to direct the beams to the same spot in the position-sensitive detector).

2. *Storing UCN on specular trajectories*

The design of the proposed experiment is inspired, to some extent, by the experiment [112] in which the storage of UCN on specular trajectories was used to search for the electric charge of the neutron ($q_{\rm n}$). However, all its parameters are improved.

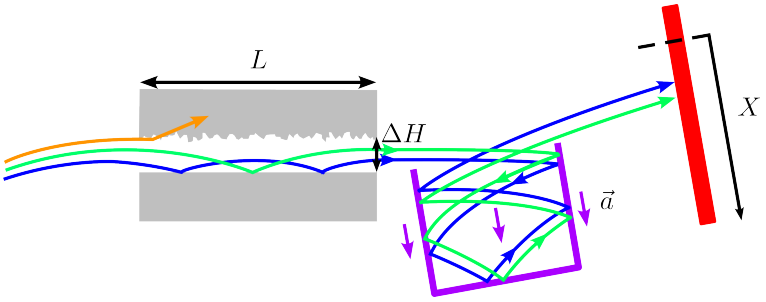

FIG. 4. A schematic of the UCN GQS experiment in reduced gravity to measure $q_{\rm n}$ or G. An incoming UCN beam enters a mirror absorber/scatterer system which is oriented such that the Earth's gravitational field is pointed nearly normal to the page. GQS with reduced gravity are populated and generate interference patterns which then enter a storage volume where an additional force is exerted on the outgoing beam, either gravitational from a large mass or electric from electrodes, both are generically indicated by $\vec{a}$. After some time in the volume, the beam leaves and reaches a detector to record the interference pattern. An element to shape and analyze the neutron's velocity may also be advantageous, depending on the available UCN spectrum.

The optical system for storing UCN on specular trajectories may be a rectangular box with specular internal walls and slits for the input and output of the UCN beam (see Fig. 4). The total storage time of UCN on specular trajectories is limited by the probability of off-specular reflections, which does not exceed $\sim 2 \cdot 10^{-3}$ for polished surfaces [113] and $\sim 5 \cdot 10^{-3}$ for diamond-like coatings [114]. For polished mirrors and a conservatively estimated frequency of wall collisions

$$\nu^{UCN}_{GQS^{reduced}} \sim 5 \text{ s}^{-1} \tag{40}$$

(which depends on the precise experimental design and the UCN spectrum), the total observation time is limited to

$$T^{UCN}_{GQS^{reduced}} < 100 \text{ s} \quad . \tag{41}$$

For simple geometry (see Fig. 2), the size of the interference pattern will increase during this interval (Eq. (41)) too much. Therefore, we will limit the observation time to such a value at which the interference patterns do not yet overlap during successive reflections from mirrors oriented (almost) perpendicular to the UCN motion trajectories. For the widths of these mirrors equal to 1 m, the longitudinal UCN velocities of 2 m/s (Eq. (31)) and the transverse UCN velocities of 10^{-3} m/s (Eq. (38)), the observation time is equal to

$$T^{UCN}_{GQS^{reduced}} \sim 20 \text{ s} \quad . \tag{42}$$

and the interference pattern size is

$$\Delta x_{\perp} = 2V^{UCN}_{GQS^{reduced}} \cdot T^{UCN}_{GQS^{reduced}} \sim 4 \text{ cm} \quad , \tag{43}$$

Simulated interference patterns are shown in Fig. 5.

3. Estimation of sensitivity of the UCN WGS interferometer to the gravitational constant G

The following sensitivity estimate is made under the most general assumptions and serves only as an initial guide. The result depends on the degree of monochromaticity of the longitudinal velocities of UCN, but not very strongly, and the window of longitudinal velocities can be quite wide. Suppose that our measurement is the difference in the interference pattern with or without an additional source mass that interacts with the neutrons only by gravitation. For the source mass being a tungsten ball with a diameter of ~ 1 m and the UCN just close to the beam, we expect an additional acceleration of $\sim 3 \cdot 10^{-7}$ g.

With the parameters presented above, ~ 10 days of statistics taking, and the phase space density of UCN available at the PF2 facility at the ILL, the sensitivity can reach a few times 10^{-3} of the value G. In view of the rather contradictory results of existing experiments [115], an independent reliable measurement with a sensitivity better than 10^{-4} may be of interest. Due to the "fine tuning" of the experimental parameters (mirror sizes, UCN storage time on specular trajectories, the number of quantum states in the interference pattern formation system, statistics collection time, use of future sources with higher UCN density, etc.), such

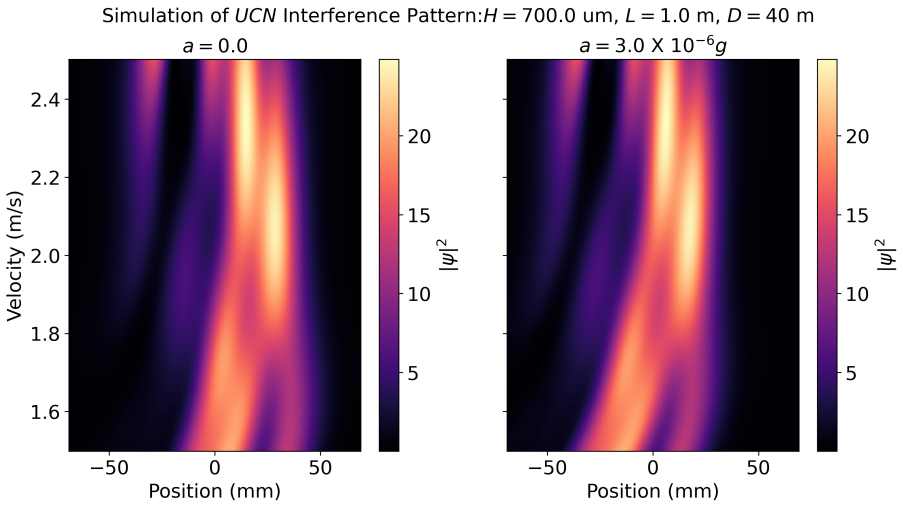

FIG. 5. Simulations of the expected interference pattern for UCN G and $q_{\rm n}$ measurements. A mirror absorber/scatterer system of length $L^{UCN}_{GQS^{reduced}} = 1$ m is used for calculations with the absorber/scatterer height of $\Delta H^{UCN}_{GQS^{reduced}} = 700$ μm. The system oriented so that the slit between the mirror and absorber/scatterer is nearly vertical, as described in the text. The exiting wave packet is propagated into free space for $D^{UCN}_{GQS^{reduced}} = 40$ m, corresponding to the $T^{UCN}_{GQS^{reduced}} = 20$ s observation time for $V^{UCN}_{GQS^{reduced}} = 2$ m/s UCNs. The effect of a gravitational field from a test mass, or the electric field of electrodes, was included with the presence of a uniform field that allows the exiting wave packet to "fall." The left plot shows the pattern without the effect of an external force and the right has an applied acceleration of $a = 3 \times 10^{-6} g$. This is 10 times higher than the proposed additional acceleration to improve the visibility the pattern's shift to more negative positions.

an increase in sensitivity seems realistic. The use of a well-known quantum system can limit some systematic errors. However, the analysis of such an experiment is a separate and extremely complex task, far beyond the scope of this work.

C. Estimation of sensitivity of the UCN WGS interferometer to a neutron electric charge $q_{\rm n}$

The same comment should be made for the case of assessing the sensitivity of this method to the presence of an electric charge on the neutron $q_{\rm n}$. In order to estimate the sensitivity of the experiment to the presence of $q_{\rm n}$, we assume that the electric field is applied along

the entire trajectory of the neutron and its intensity is $\sim 10^4$ V/cm. On the one hand, the electrodes cannot be placed near the mirrors (otherwise, the shadow effect will occur, as the electrodes would be found in the UCN beam). However, the field intensity along that part of the neutron trajectory where the interference pattern is small can be many times higher. Therefore, our sensitivity estimate is very conservative and is $q_{\rm n} \sim 10^{-22}\ e$. At the same time, all the arguments about the possible "fine-tuning" of the parameters and the further increase in sensitivity by one or two orders of magnitude remain valid. In view of the fact that the best limit on the $q_{\rm n}$ value today is $\sim 10^{-21}\ e$ [116], our estimate seems very promising.

If one decides to take more concrete steps in these directions, the exact experimental design must be developed, the sensitivity optimized, and systematic effects studied theoretically and experimentally. [2]

IV. A POSSIBLE MEASUREMENT OF THE WGS OF HYDROGEN AND ITS GRAVITATIONAL SHIFT

A. Optimization of experiments with the WGS of H

The effective critical energies of all materials for Hare quite small, and even smaller for heavier atoms [30, 73, 117–119]. Therefore, we are interested in a material with a maximum effective critical energy. Among those considered in ref. [30], we select Silica. We ignore the liquid-helium surface on the curved mirror, due to experimental difficulties.

The density in the phase space of the H beam can be high (compared to neutron beams). However, the angular spread in the interference pattern is small because of these low effective critical energies. Therefore, we prefer quite a lot of quasi-classical bounces and only a few WGS. This choice will provide a sufficiently informative interference pattern with a large number of interference fringes. For this choice, the requirements for the spatial resolution of the H detector are not too demanding.

A motivation for the informative interference pattern is the possibility of extracting un-

[2] An interferometer of this type can also be designed for ultracold atoms, however, the analysis of this possibility is far beyond the scope of this article.

precedentedly precise and detailed information about the QR process. Thus, for

$$\beta^H_{WGS} \sim 10 \tag{44}$$

and

$$\gamma^H_{WGS} \sim 3 + N \tag{45}$$

(N is the number of exited WGS),

$$E^H_{lim} \sim 1.2 \cdot 10^{-11} \text{ eV} \quad . \tag{46}$$

The precise simulations in the following will illustrate the sensitivity to these parameters.

Eqs. (1a) to (1d), (10) and (44) to (46) result in

$$\tau^H_{WGS} = \tau^H_{GQS} \frac{\gamma^H_{WGS} \cdot E^H_{GQS}}{E^H_{lim}} \sim 2.5 \cdot 10^{-4} \text{ s} \quad . \tag{47}$$

Eqs. (8) and (47) result in

$$a^H_{WGS} \sim g \cdot \left(\frac{\tau^H_{GQS}}{\tau^H_{WGS}} \right)^{1.5} \sim 9.0 \cdot 10^1 \text{ m/s}^2 \quad . \tag{48}$$

To have the mirror compatible with the GRASIAN setup [81, 82] we select the same mirror length as that in the GQS experiments:

$$L^H_{WGS} = 0.3 \text{ m} \quad . \tag{49}$$

Eqs. (45), (47) and (49) result in

$$V^H_{WGS} \sim \frac{L^H_{WGS}}{\beta^H_{WGS} \cdot \tau^H_{WGS}} \sim 1.2 \cdot 10^2 \text{ m/s} \quad . \tag{50}$$

Eqs. (48) and (50) result in

$$R^H_{WGS} \sim \frac{(V^H_{WGS})^2}{a^H_{WGS}} \sim 1.6 \cdot 10^2 \text{ m} \quad . \tag{51}$$

The ratio of the magnitudes of gravitational and centrifugal (Eq. (48)) accelerations ,

$$\frac{g}{a^H_{WGS}} \sim 1.1 \cdot 10^{-1} \quad , \tag{52}$$

is "huge" compared to the $\sim 10^{-5}$ value measured in the neutron experiment [29].

This large magnitude of the gravitational effect makes measuring the gravitational shift of the WGS experimentally accessible. It is enough to simply compare the results of the measurement with the reflective surface of the cylindrical mirror directed (almost) downward with the results of the measurement with the reflective surface of the cylindrical mirror (almost) upward. The remaining parameters of the experiments are identical.

B. Simulation of an H WGS interference pattern

The optimal velocity of H in Eq. (50) is close to the characteristic velocities of the H beam in the GQS experiment performed within the framework of the GRASIAN project [81, 82]. So we simply use the optimum parameters to simulate the interference pattern that we would like to measure:

$$L^H_{WGS} = 0.3 \text{ m} \quad ; \quad V^H_{WGS} = 1.2 \cdot 10^2 \text{ m/s} \quad ; \quad R^H_{WGS} = 1.6 \cdot 10^2 \text{ m} \quad . \tag{53}$$

The efficiency of the critical energy of the mirror as a "filter" of atomic WGS is limited because the lifetimes of WGS with energy above the critical energy do not decrease sharply. Therefore, we will add one more element to the experimental setup: an additional scatterer/absorber in the initial part of the mirror. By changing the height of the scatterer/absorber above the mirror, it is possible to change the number of WGS that can pass through the slit with small losses. We are not interested in an "absolutely sharp" cut-off of the spectrum of WGS. Therefore, here and in all similar cases below, we will choose the absorber/scatterer length equal to the length of one quasi-classical bounce, or L_{WGS}/β_{WGS}.

To resolve the peaks seen in the interference pattern on the left of Fig. 6 and the most prominent peaks of the more intricate pattern seen on the right of Fig. 6, the chopper time window should not exceed ~ 3 ms, and the spatial resolution of the position sensitive detector should not be worse than ~ 300 μm. To resolve the fine structure of this interference pattern, the tighter constraints of a ~ 0.5 ms time window and ~ 50 μm position resolution are necessary. In the following, we will give more details about how the measurement will be performed simply because it is already planned for the near future.

C. A scheme of an H WGS experiment

In order to measure a maximal gravitational shift, we need a set of differential measurements that allows us to measure the WGS while maximizing the differential value of g/a^H_{WGS}, and measure with best precision. For our cylindrical mirror with a very large radius of curvature, this means that the cylindrically polished side has to face upward or downward. This constellation will be henceforth referred to as the "upwards" or "downwards-falling" mirror constellation, depending on the orientation of the polished surface. If the symmetry axis of the cylinder is parallel to the direction of gravity, the WGS formation would be decoupled

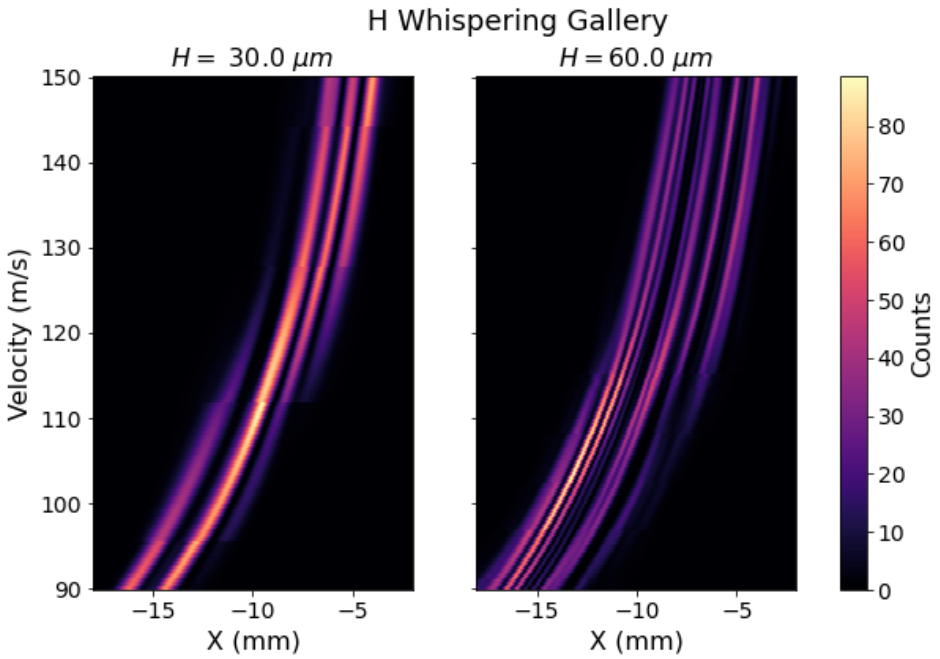

FIG. 6. Simulations of the expected interference pattern for the optimal parameters, a radius $R^H_{WGS} = 160$ m and a length $L^H_{WGS} = 30$ cm. Two scenarios are shown, each with an absorber/scatterer of length $(L_A)^H_{WGS} = 5$ cm placed on the mirror as in figure $\Delta H_{WGS} = 70$ μm above the beginning of the mirror. An incident plane wave is assumed to enter the gallery with no incidence angle and is propagated through the gallery by solving the Schrödinger Equation. The wave packet at the exit of the gallery is then propagated through a free fall region of length $D^H_{WGS} = 5$ m. This image does not consider the velocity distribution of the H beam, nor the resolution effects of the detection system. The gravitational acceleration points in the negative direction in position space, and the origin corresponds to the edge at the exit of the gallery.

from gravitational effects (to a good approximation with a strictly downwards facing gravitational field). We will call this the "free" or "decoupled" case. In the "falling" case, we have the total acceleration $a_{WGS} \pm g$, depending on the upward / downward orientation of the polished surface.

For the measurement of the gravitational shift we want to measure in the "falling" constellation, and compare interferences of upward-oriented mirror surface to the interference pattern when the mirror faces downward. This measurement allows prototyping experiments with $\overline{\text{H}}$ and evaluation of the sensitivity to gravitational shift as well as the accuracy of the estimation of this value.

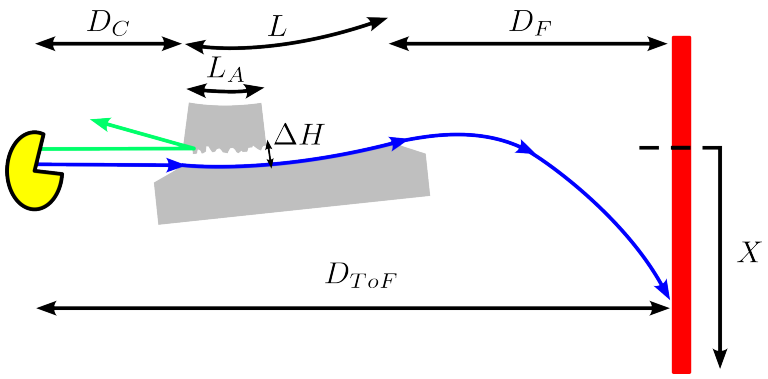

FIG. 7. A schematic of the H WGS experiment. A collimated beam of H enters the system through a chopper, placed a distance D_C away from the entrance of the mirror, which enables the measurement of the velocity of H atoms by the time of flight (ToF) method. The beam then enters the mirror absorber/scatterer system. Lower energy WGS can pass through the initial section where an absorber/scatterer of length L_A is placed a height ΔH above the mirror, while higher WGS are rejected. The lower WGS then propagate along the surface and interfere with each other until reaching the end of the mirror, which has a total length L. The exiting beam enters a free fall region where a time and position sensitive detection system is place a distance D_F from the exit of the mirror. The position of the H atom on the detector is denoted as X.

D. A cryogenic beam of slow velocity H for WGS measurements

The measurement of the WGS of H will take place at the Marietta Blau Institute (MBI) in Vienna with the cold H beamline developed at ETH Zurich in recent years [81, 82]. The setup is being prepared for the observation of GQS at the time of writing this article.

The beam of atomic H is generated by dissociating H_2 molecules in a microwave cavity and directing the H plasma with a Teflon nozzle to a copper piece attached to the cold head in an optimized geometry [120]. By collisions with the cold nozzle, H is cooled to ~ 6 K. A chopper allows one to determine the longitudinal velocity of the beam by time-of-flight measurement, selecting the slow tail of the velocity distribution [81, 82].

In parallel, a new H source operating at the temperature of ~ 100 mK has been developed in Turku by members of the GRASIAN collaboration [121, 122]. Such a source would greatly increase the number of atoms with velocities below 100 m/s, substantially enhancing the fraction of atoms suitable for WGS measurement and opening the way to higher-contrast

interference and improved statistics in future experiments.

E. Resolution of the H WGS interference pattern

The time resolution is defined by the opening time of the chopper, which, at the moment, is $\sim$ 5 ms. The current detection scheme of H achieves a spatial resolution of $\sim$ 200 μm [81, 82].

A new chopper will be used, with an opening time of 0.5-3.0 ms, improving the resolution; the actual value should match the spatial resolution obtained. The width of the laser beam at the smallest point of detection, which is $\sim$ 200 μm at the moment, is already sufficient to measure the major features of the WGS of H. Improvement of the spatial resolution is much more complicated than improvement of the time resolution, which depends only on the chopper opening window (and to a very small part also on the duration of the laser pulse, which is negligible). However, it is possible to improve the resolution using alternative detection methods (for example, with microchannel plates), which could yield a resolution sub- 200 μm.

F. A demonstration of the GQS of H using the interference method

Using the same installation as described in the previous sections and the same method as described in Section III A for neutrons, one can prove the existence of GQS of H. The only difference consists of a slightly different flight path available ($\sim$ 5 m), a slightly different spatial resolution of the detector ($\sim$ 200 μm), and a slightly different velocity range (see Fig. 8).

V. MEASUREMENT OF THE WGS OF ANTIHYDROGEN AND ITS GRAVITATIONAL SHIFT

WGS and GQS of $\overline{\mathrm{H}}$are of interest for an investigation of the gravitational interaction of antimatter [70–73]. The argument can be made that the gravitational interaction between matter and antimatter is well known from tests of the equivalence principle with objects that contain antimatter, i.e., nucleons. Kostelecky et al. [79] discuss how the constraints

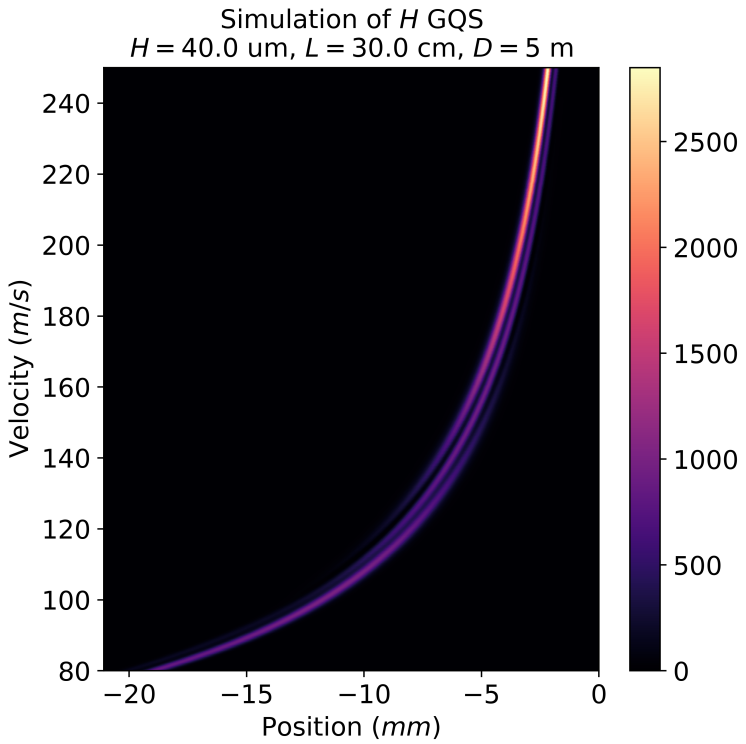

FIG. 8. A simulation of the interference pattern generated by H propagating through a mirror-absorber/scatterer system of the same type as proposed for the VCN GQS measurement. The length of the system is $L^H_{GQS} = 30$ cm and the absorber/scatterer height is $\Delta H^H_{GQS} = 40$ μm. H enters a free fall region of length $D^H_{GQS} = 5$ m after leaving the mirror.

from these experiments can be evaded. The first result of a gravitational interaction test with $\overline{\text{H}}$ has recently been achieved in [88].

A. Optimization of experiments with the WGS of $\overline{\text{H}}$

A specific feature of experiments with $\overline{\text{H}}$ is the difficulty in producing them sufficiently cold. Therefore, we will use Silica for the mirror, a material with high effective critical energy, as we did in the case of H. An even larger effective critical energy for the mirror material would be advantageous because, on the one hand, it would expand the range of acceptable $\overline{\text{H}}$ velocities and, on the other hand, it would increase the number of interference fringes, thereby increasing the accuracy of gravitational shift measurements. Since the list of materials for which this value is known is very limited, it is highly likely that such materials

exist and could be used to fabricate a mirror. Therefore, searching for such materials is an important task. For now, we use Silica and evaluate the maximum values $V^{\bar{H}}_{WGS}$, at which the experiment is still feasible.

As the acceptable velocity of $\overline{\mathrm{H}}$ increases with increasing mirror length, we set it to a large value [3]:

$$L^{\bar{H}}_{WGS} \sim 1 \text{ m} \quad . \tag{54}$$

The acceptable velocity of $\overline{\mathrm{H}}$ also increases with increasing mirror radius $R^{\bar{H}}_{WGS}$. However, a precision mirror with a too large radius of curvature is difficult to manufacture, and the curvature of the mirror surface would not be maintained with sufficient accuracy. Moreover, it cannot be too large to avoid a direct view through the slit between the mirror and the scatterer/absorber. To reduce this effect, the length of the absorber/scatterer must be increased when observing a large number of quantum states. All of these factors are difficult to quantify simultaneously, so we rely on our previous experience with mirrors.

$$R^{\bar{H}}_{WGS} \sim 10^4 \text{ m} \quad . \tag{55}$$

To increase effective critical energy, we prefer a limited number of quasi-classical bounces. A comfortable number of quasi-classical bounces is, say:

$$\beta^{\bar{H}}_{WGS} \sim 5 \quad . \tag{56}$$

However, we will simulate the interference pattern up to maximum values of $V^{\bar{H}}_{WGS}$ thus exploring also the regime of $\beta^{\bar{H}}_{WGS} \sim 1$.

To observe an interference pattern with a significant number of interference lines, the system should provide at least a few WGS:

$$\gamma^{\bar{H}}_{WGS} \sim 3 + 2 \quad . \tag{57}$$

This combination of parameters results in the following set of effective critical energy $E^{\bar{H}}_{lim}$, acceleration $a^{\bar{H}}_{WGS}$, and velocity $V^{\bar{H}}_{WGS}$ for an experiment with $\overline{\mathrm{H}}$:

$$E^{\bar{H}}_{lim} \sim 2.0 \cdot 10^{-10} \text{ eV}; \quad a^{\bar{H}}_{WGS} \sim 5.4 \cdot 10^3 \text{ m/s}^2; \quad V^{\bar{H}}_{WGS} \sim 7.4 \cdot 10^3 \text{ m/s} \quad . \tag{58}$$

[3] Some increase in the mirror length is possible and this option should be carefully analyzed if the proposed method is to be considered for a specific project.

The measurement can be performed with $\overline{\mathrm{H}}$ of thermal velocities, or several times larger (we will evaluate in Section V C up to what velocity of $\overline{\mathrm{H}}$ the feasible range can be, in principle, extended). For the optimal velocity of $V_{WGS}^{\bar{H}} \sim 7.4 \cdot 10^3$ m/s, the gravitational shift is $\sim 1.8 \cdot 10^{-3}$. It can be measured with a few percent accuracy. Smaller velocities of the $\overline{\mathrm{H}}$ would be an advantage. Higher velocities of $\overline{\mathrm{H}}$ can also be considered; however, the gravitational shift decreases quadratically with increasing velocity. Fabrication of required mirrors is feasible.

In order to avoid extremely precise absolute measurements, it seems reasonable to measure the WGS of $\overline{\mathrm{H}}$ and H using the same mirror and compare the results. Theoretical corrections responsible for the small difference in QR of $\overline{\mathrm{H}}$ and H should then be introduced.

B. A scheme of an $\overline{\mathrm{H}}$ WGS experiment

To propose an experimental setup for $\overline{\mathrm{H}}$, one should keep the following factors in mind: the angular spread of $\overline{\mathrm{H}}$ at the mirror exit is very small due to the very large longitudinal velocities of $\overline{\mathrm{H}}$ and the very low transverse velocities. Therefore, the experimental setup possible with n and H (Fig. 7) is not applicable directly here.

However, another option is possible. When touching the mirror surface, the $\overline{\mathrm{H}}$ is annihilated and the signal from such an event (charged pions) can be registered in a position-sensitive detector. For this reason, the "useful signal" that we simulate in Section V C is the flow of $\overline{\mathrm{H}}$ into the mirror surface. Another difference is that the longitudinal velocity of the $\overline{\mathrm{H}}$ atom is not set by the chopper; the spectrum is monochromatic or is set by the moment of release of $\overline{\mathrm{H}}$ from the trap (depending on the specific implementation of the experiment).

The last "free parameter" in this experimental setup (Fig. 9) is the height $\Delta H_{WGS}^{\bar{H}}$ of the absorber/scatterer above the mirror. By increasing $\Delta H_{WGS}^{\bar{H}}$, we can increase the number of observed interference fringes and thus increase the sensitivity of the experiment to measuring gravitational acceleration. However, this increase is limited by the spatial resolution of the position-sensitive detector of $\overline{\mathrm{H}}$ annihilation, the direct view through the slit mirror-absorber/scatterer as well as by the decrease in the lifetime of the WGS with increasing quantum state number.

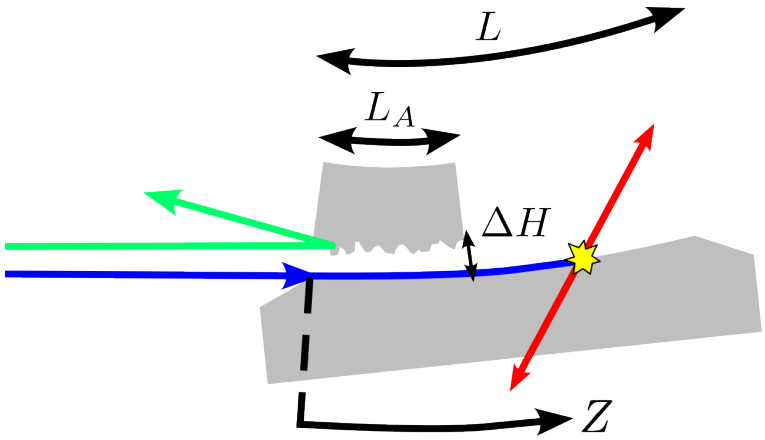

FIG. 9. A schematic of the $\overline{\text{H}}$ WGS experiment. A collimated monochromatic beam of $\overline{\text{H}}$ enters the mirror absorber/scatterer system. Like with the H WGS set-up before, an absorber/scatterer of length L_A is placed a height ΔH above the mirror and filters out higher energy WGS. The surviving WGS propagate along the surface and interfere over the mirror of length L. The $\overline{\text{H}}$ atoms which are not reflected by the Casimir-Polder interaction will reach the surface and annihilate. The position Z of this annihilation event is taken as the signal and is experimentally determined by recording the trajectories of the annihilation products. The predicted annihilation rate can be taken as the probability current of the $\overline{\text{H}}$ wave function at the mirror surface,

C. Simulation of an $\overline{\text{H}}$ WGS interference pattern

The parameters used for the simulation are:

$$L^{\bar{H}}_{WGS} = 1 \text{ m}; \quad R^{\bar{H}}_{WGS} = 10^4 \text{ m}; \quad V^{\bar{H}}_{WGS} = 7.4 \cdot 10^3 \text{ m/s} \quad . \tag{59}$$

A characteristic slit size $l^{\bar{H}}_{WGS}$ is:

$$l^{\bar{H}}_{WGS} \sim 1.5 \ \mu\text{m} \quad . \tag{60}$$

To allow for N excited WGS, one should set the slit to the height:

$$\Delta H^{\bar{H}}_{WGS} \sim l^{\bar{h}}_{WGS} \cdot (3 + N) \quad . \tag{61}$$

The interference pattern simulated in Fig. 10, can be measured with velocities of $\overline{\text{H}}$ up to $\sim 10^5$ m/s. They are an order of magnitude lower than those available in the GBAR experiment [123]. Moreover, the loss of $\overline{\text{H}}$ atoms increases rapidly with increasing velocity. The flux of $\overline{\text{H}}$ decreases by an order of magnitude if the velocity of $\overline{\text{H}}$ increases by a factor of

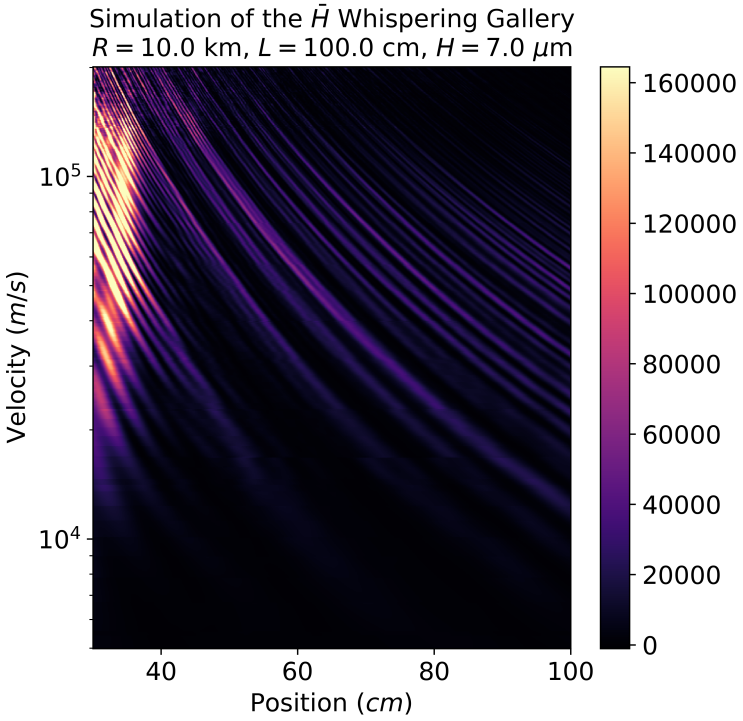

FIG. 10. A simulation of the annihilation rate of $\bar{H}$ on the surface of a WGS mirror with the parameters in Eq. (59) and a wide range of velocities. An absorber/scatterer at a height $\Delta H^{\bar{H}}_{WGS} \sim 7$ μm allows 62 states to be populated for 200.000 m/s and 4 states for 5000 m/s in the absorber/scatterer region. The spatial resolution of the $\overline{\mathrm{H}}$ annihilation detector needed to measure WGS with the $\overline{\mathrm{H}}$ velocity of 200.000 m/s is ~ 1 mm, and it is ~ 5 mm for the $\overline{\mathrm{H}}$ velocity of 5000 m/s.

~ 2. "Fine tuning" of the experimental parameters ($L^{\bar{H}}_{WGS}$, $R^{\bar{H}}_{WGS}$, $\Delta H^{\bar{H}}_{WGS}$, mirror material, etc.) for specific beam parameters is possible. However, smaller velocities of $\overline{\mathrm{H}}$ are always an advantage.

In principle, it is possible to perform a similar experiment even with $\overline{\mathrm{H}}$ velocities of $\sim 10^6$ m/s. This requires using the material with the highest critical energy, liquid helium. Since coating the surface of a cylindrical mirror with a thick layer of helium with stable, well-controlled, and consistent properties seems unrealistic, the mirror surface must be flat. To achieve the GQS/WGS effect, an additional force must be added, pressing the $\overline{\mathrm{H}}$ to the helium surface due to a magnetic field gradient. We may optimize this possibility if it is of practical interest. Unfortunately, it will not be an elegant, simple solution like most of the proposals in this article, but rather a large and expensive cryogenic device with superconductors to generate the magnetic gradient. In addition, the gravitational shift

decreases quadratically and becomes too small to be measured reliably.

VI. GQS OF HYDROGEN AND ANTIHYDROGEN ON A "FALLING MIRROR"

As noted above, the storage time of H and $\overline{\mathrm{H}}$ on the plane, due to QR from the surface, is limited to ~ 1 s. This is much longer than the observation times of the UCN in existing experiments, which can dramatically increase the accuracy of quantum gravitational spectroscopy and interferometry. Because the atoms stored in GQS interact with the surface in a well-known way, this interaction can be taken into account very accurately. This circumstance opens up the potential for Doppler-free optical and hyperfine spectroscopy of such atoms, since their effective velocities in the direction perpendicular to the plane (the velocity distribution in the lowest GQS) are record low.

It is of interest to consider the possibility of even longer storage of atoms on the surface and even more precise spectroscopy and interferometry. This can be achieved by placing the atoms in reduced gravity. In the laboratory, this effect can be achieved most simply by tilting the magneto-gravitational trap (MGT) [124]. However, it will be the same when the mirror falls with almost gravitational acceleration and when the experiment is actually placed in reduced gravity. In all these cases, we will simply consider the reduced gravitational acceleration $g^{(H,\bar{H})}_{GQS^{reduced}}$.

To understand the effect of reduced gravity, let us reproduce the dependences of all parameters on the value of $g^{(H,\bar{H})}_{GQS^{reduced}}$:

$$E^{(H,\bar{H})}_{GQS^{reduced}} \sim (g^{(H,\bar{H})}_{GQS^{reduced}})^{\frac{2}{3}}, l^{(H,\bar{H})}_{GQS^{reduced}} \sim (g^{(H,\bar{H})}_{GQS^{reduced}})^{-\frac{1}{3}}, \tau^{(H,\bar{H})}_{GQS^{reduced}} \sim (g^{(H,\bar{H})}_{GQS^{reduced}})^{-\frac{2}{3}}. \quad (62)$$

The lifetime $t^{(H,\bar{H})}_{GQS^{reduced}}$ of H and $\overline{\mathrm{H}}$ in GQS, due to QR from the surface, is proportional to

$$t^{H,\bar{H}}_{GQS^{reduced}} \sim (g^{(H,\bar{H})}_{GQS^{reduced}})^{-\frac{4}{3}} \quad . \quad (63)$$

The significant increase in storage time is easy to understand in quasi-classical approximation: with a decrease in gravity, it increases both by reducing the frequency of bounces on the surface and by increasing the wavelength of the atom.

At the same time, the precision measurement of the spectrum of GQS (in reduced gravity) $\Delta E^{(H,\bar{H})}_{GQS^{reduced}}/E^{(H,\bar{H})}_{GQS^{reduced}}$, which in a rough approximation is proportional to the number of

quasi-classical bounces, quickly improves:

$$\frac{\Delta E^{(H,\bar{H})}_{GQS^{reduced}}}{E^{(H,\bar{H})}_{GQS^{reduced}}} \sim \frac{t^{H,\bar{H}}_{GQS^{reduced}}}{\tau^{H,\bar{H}}_{GQS^{reduced}}} \sim (g^{(H,\bar{H})}_{GQS^{reduced}})^{\frac{2}{3}} \quad . \tag{64}$$

In addition to the proven significant increase in the accuracy and sensitivity of spectroscopic and interferometric measurements, the requirements for optical elements in such experiments are greatly simplified. Since the characteristic sizes of quantum states become much larger, the requirements for surface roughness, the relative accuracy of mirror and absorber/scatterer installation, the resolution of position-sensitive detectors, etc. are significantly lower.

VII. WGS OF MUONIUM

A. Optimization of an experiment with the WGS of Muonium

We turn to a discussion of WGS of Muonium (Mu). Kosteleczky et al. [79] discuss a non-standard Hamiltonian with new terms that depend on particle species. Investigations of the new coupling constants to higher generation particles are rare and of independent interest. The authors expect that the new coupling constants increase with fermion mass. When considering the feasibility of measuring the WGS of Mu, there are several limitations and advantages that should be taken into account.

On the "limitations" side, the Mu lifetime is short:

$$\tau^{Mu} \sim 2.2 \cdot 10^{-6} \text{ s} \quad , \tag{65}$$

therefore, the observation time of the WGS of Mu (τ^{Mu}_{WGS}) cannot exceed this value substantially.

However, the use of sources of Mu at cryogenic temperatures [125] or of the novel beam of Mu produced from superfluid helium [90] with a velocity of

$$V^{Mu}_{WGS} \sim 2.2 \cdot 10^{3} \text{ m/s} \tag{66}$$

combined with the planned High Intensity Muon Beamline (HIMB) upgrade at PSI [126] could allow the observation of WGS. This velocity is even significantly lower than that of $\overline{\text{H}}$ discussed in Section V.

In addition, due to the small mass of Mu,

$$m^{Mu} \sim 0.113 \cdot m^{n,H,\bar{H}} \quad , \tag{67}$$

the effective critical energy of materials for Mu is much larger than their effective critical energy for the H and $\overline{\mathrm{H}}$ atoms.

On the one hand, large effective critical energies simplify the observation of the WGS of Mu, and relax constraints on Mu velocities. This is particularly useful if the goal is to obtain a complex interference pattern and investigate in detail the QR phenomenon itself. On the other hand, the relative value of the gravitational shift is then much smaller. Therefore, we will aim to optimize the experimental parameters to simplify the observation of the gravitational shift.

In addition to that, Mu emitted from superfluid helium [127, 128] can be considered monochromatic to some extent (we will illustrate this statement quantitatively in Section VII B):

$$\delta V^{Mu} \sim 5 \cdot 10^{1} \text{ m/s} \quad , \tag{68}$$

and the phase space density of the Mu beam is quite large.

For

$$\tau^{Mu}_{WGS} = 3 \cdot \tau^{Mu} \quad , \tag{69}$$

the mirror length [4] is

$$L^{Mu}_{WGS} \sim V^{Mu}_{WGS} \cdot \tau^{Mu}_{WGS} \sim 1.5 \cdot 10^{-2} \text{ m} \quad . \tag{70}$$

We begin optimizing this experiment by comparing it with the measurement of the magnetic shift of the neutron WGS [29]. In this short measurement, the relative contribution of an additional force was $\sim 10^{-5}$. In a dedicated experiment, the sensitivity can greatly increase; however, we start optimizing the Mu experiment from this value. So, we get the first condition:

$$a^{Mu}_{WGS} \sim 10^{6} \text{ m/s}^2 \quad . \tag{71}$$

Thus, the characteristic time of formation of the WGS is (Eq. (8,67)):

$$\tau^{Mu}_{WGS} \sim 9.3 \cdot 10^{-7} \text{ s} \quad . \tag{72}$$

[4] We accept that only a small fraction of the beam can reach the exit of the mirror but try to maximally increase the sensitivity using this parameter (L^{Mu}_{WGS}).

Note that the formation time of the quantum state τ_{WGS}^{Mu} is shorter than the lifetime of Mu, τ^{Mu}, so the number of quasi-classical bounces (Eq. 12) is acceptable:

$$\beta_{WGS}^{Mu} \sim \frac{\tau^{Mu}}{\tau_{WGS}^{Mu}} \sim 2.3 \quad . \tag{73}$$

The mirror radius is comfortable for the mirror manufacturing (Eqs. (6,66,72)):

$$R_{WGS}^{Mu} \sim 4.8 \text{ m} \quad . \tag{74}$$

The only parameter that is too large is the number of WGS. For β_{WGS}^{Mu} (Eq. (73)) bounces on Silica, it is

$$\gamma_{WGS}^{Mu} \sim 8.6 \cdot 10^2 \quad . \tag{75}$$

Therefore, the choice of mirror material does not matter and we have to limit the number of WGS in a different way. As we did for H and $\overline{\text{H}}$, a short absorber/scatterer should be installed in the Mu experiment above the initial part of the mirror with a slit size ΔH_{WGS}^{Mu}:

$$\Delta H_{WGS}^{Mu} \sim l_{WGS}^{Mu} \cdot (3 + N) \quad , \tag{76}$$

where

$$l_{WGS}^{Mu} \sim 5.6 \cdot 10^{-7} \text{ m} \tag{77}$$

and N is the number of excited WGS.

We prefer a large number of WGS because such a choice, on the one hand, allows us to increase statistics, and, on the other hand, it increases the number of interference bands and, thus, increases the sensitivity of the experiment. However, with too many WGS, the number of interference lines might be too large, the distance between them might be too small, and they might not be spatially resolved in the detector.

Although all the parameters of the problem are quite comfortable for observing the WGS of Mu, measuring the gravitational shift of the WGS of Mu is much more challenging. The relative shift is

$$\frac{g}{a_{WGS}^{\text{Mu}}} \sim 10^{-5} \quad . \tag{78}$$

This value (Eq. 78) matches exactly the sensitivity of the short neutron experiment [29]. Therefore, achieving the same sensitivity in the Mu experiment is not fundamentally difficult. However, unlike the neutron experiment, in which the direction of the additional force was reversed, in the case of measuring a gravitational shift of the WGS of Mu, one needs to reverse

the orientation of the mirror. This means that one must ensure the mirror adjustment and control with corresponding accuracy, which is an extremely challenging task. In any case, prototyping this experiment with neutrons seems like a necessary preliminary step because all the parameters of this task are typical for neutron experiments, and the neutron fluxes are also high. For example, such an experiment can be performed at the PF1B facility at the ILL [129].

B. Simulation of a Mu WGS interference pattern

Here, we summarize the experimental parameters for the WGS of Mu (Eqs. (66,70,74,76)):

$$V_{WGS}^{Mu} \sim 2.2 \cdot 10^3 \; m/s; L_{WGS}^{Mu} \sim 1.5 \cdot 10^{-2} \text{ m}; R_{WGS}^{Mu} \sim 4.8 \text{ m}; \Delta H_{WGS}^{Mu} \sim 5.6 \cdot 10^{-7} \cdot (3+N) \text{ m}. \tag{79}$$

The simulation results are shown in Figs. 11 and 12.

C. A scheme of a Mu WGS experiment

The scheme for WGS formation is similar to that used for H and $\overline{\text{H}}$. However, the detection scheme of Mu would differ from the first and second cases. Unlike H, both the lifetime of Mu is too short and the angular spread of Mu is too small to be analyzed using a position-sensitive detector installed a large distance from the edge of the mirror. Unlike $\overline{\text{H}}$, measuring the annihilation points of Mu in the mirror also does not work. If the mirror is magnetic, the spin rotation of Mu upon contact with the mirror may allow the WGS pattern to be detected. However, a detection method requires more serious analysis and is not clear to us at the moment.

VIII. WGS OF POSITRONIUM

When considering the possibility of measuring the WGS of Ps, several factors should be considered.

First, since the mass of Ps is much smaller than the mass of Mu, the probability of QR and the effective critical energy are even higher. Therefore, we would use the same

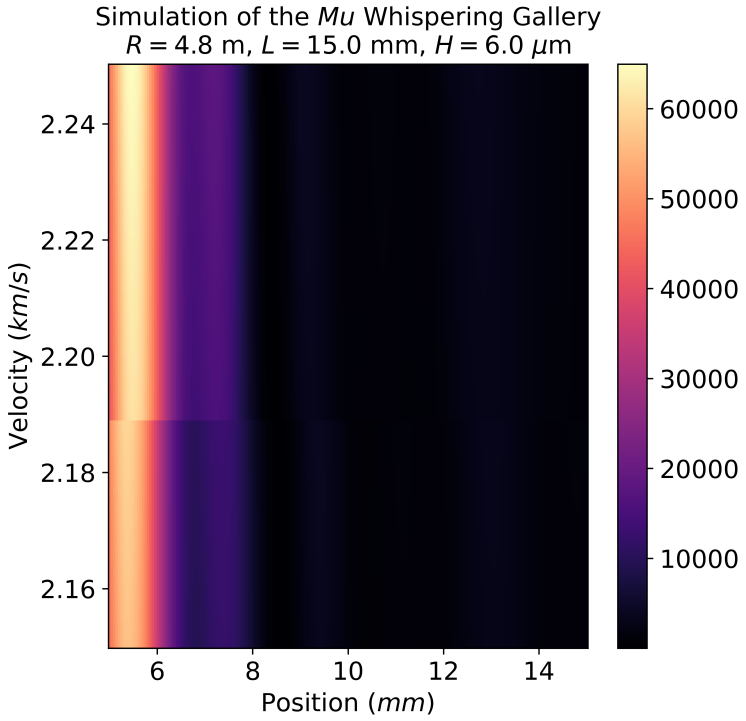

FIG. 11. A simulation of the Mu current into the surface of the WGS mirror with the parameters in Eq. 79. 9 states contribute to the pattern due to the presence of an absorber/scatterer of length $L_a = 5$ mm at the beginning of the mirror. The decay of Mu is taken into account. Only the region after the absorber/scatterer is presented since it's almost independent on precisely setting the ΔH^{Mu}_{WGS} value, thus more reliable to simulate.

experimental scheme as in the case of Mu, i.e., excess excited WGS are removed using an absorber/scatterer.

Second, the lifetime of Ps in the ground state is even shorter than the lifetime of Mu. However, the lifetime of the excited quantum state increases rapidly with increasing quantum number. This circumstance can be understood as follows: with an increasing quantum number, the average distance between the electron and positron increases, the overlap integral of their wave functions decreases, and, accordingly, the probability of annihilation decreases. For example, for the quantum state $n = 33$, the lifetime is

$$\tau^{Ps,n=33} \sim 10^{-5} \text{ s} \quad . \tag{80}$$

A characteristic velocity of available Ps beams is [130, 131]

$$V^{Ps} \sim 5 \cdot 10^4 \text{ m/s} \quad . \tag{81}$$

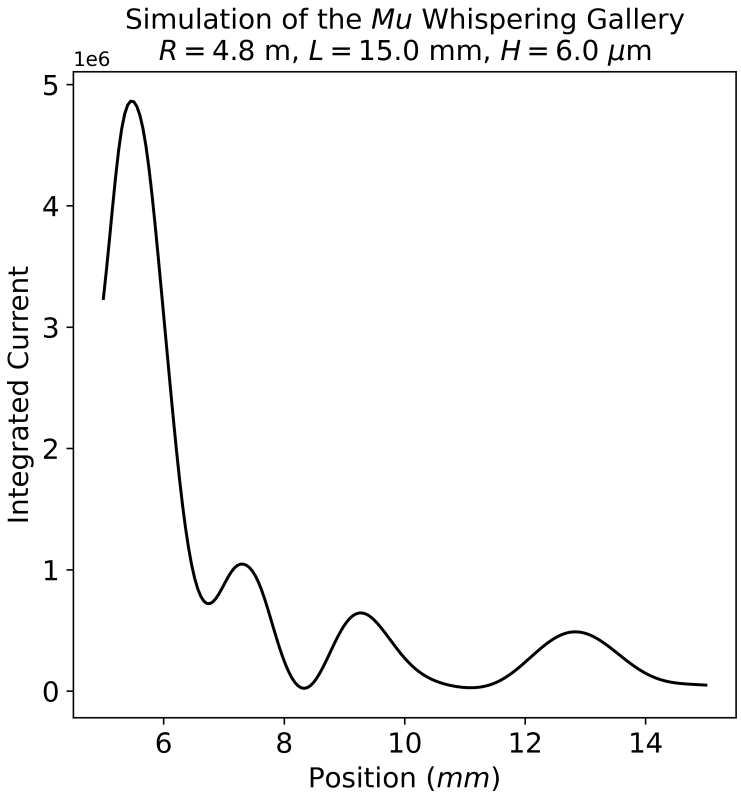

FIG. 12. The Mu current into the mirror calculated in Fig. 11 integrated over the expected velocity spectrum. The decay of Mu is taken into account. One can see that the assumption of a "monochromatic beam" (Eq. 68) is valid, and the interference contrast is very high.

Assuming that the time of flight of the Ps over the mirror ($t_{WGS}^{Ps,n=33} \sim L_{WGS}^{Ps,n=33}/V^{Ps}$) is equal to the lifetime $\tau^{Ps,n=33}$, the length of the mirror is

$$L_{WGS}^{Ps,n=33} \sim 0.5 \text{ m} \quad . \tag{82}$$

Based on these values, we will optimize the experimental design to increase the chances of observing a gravitational shift of Ps.

To decrease a relative gravitational shift, we prefer a small number of quasi-classical bounces:

$$\beta_{WGS}^{Ps,n=33} \sim 3 \quad . \tag{83}$$

Then the time of formation of the WGS of Ps is

$$\tau_{WGS}^{Ps,n=33} \sim t_{WGS}^{Ps,n=33}/\beta_{WGS}^{Ps,n=33} \sim 3.3 \cdot 10^{-6} \text{ s}, \tag{84}$$

and the acceleration is

$$a_{WGS}^{Ps,n=33} = 1.8 \cdot 10^6 \text{ m/s}^2 \quad , \tag{85}$$

and the relative gravitational shift is

$$\frac{g}{a_{WGS}^{Ps,n=33}} \sim 5.5 \cdot 10^{-6} \quad . \tag{86}$$

Note that this value (86) is as large (as small) as the sensitivity $\sim 10^{-5}$ of the neutron test experiment [29] or the estimated effect in the experiment with Mu (Eq. 78).

The radius of the mirror $R_{WGS}^{Ps,n=33}$, which corresponds to the velocity (Eq. (81)) and acceleration (Eq. (85)) of Ps, is equal to

$$R_{WGS}^{Ps,n=33} \sim 1.4 \cdot 10^3 \text{ m} \quad . \tag{87}$$

One significant simplification of such an experiment is that the size of the slit to shape the WGS is relatively large due to the small mass of Ps. The characteristic slit size is:

$$l_{WGS}^{Ps,n=33} \sim 9.8 \cdot 10^{-6} \text{ m} \quad . \tag{88}$$

For

$$\gamma_{WGS}^{Ps,n=33} \sim 10 \quad , \tag{89}$$

it is

$$\Delta H_{WGS}^{Ps,n=33} \sim 9.8 \cdot 10^{-5} \text{ m} \quad . \tag{90}$$

A. Simulation of a Ps WGS interference pattern

Let us summarize the characteristic parameters of the problem:

$$n = 33; V_{WGS}^{Ps,n=33} \sim 5{\cdot}10^4 \text{ m/s}; L_{WGS}^{Ps,n=33} \sim 0.5 \text{ m}; g/a_{WGS}^{Ps,n=33} \sim 5.5{\cdot}10^{-6}; R_{WGS}^{Ps,n=33} = 1.4{\cdot}10^3 \text{ m}. \tag{91}$$

The simulation results are presented in Fig. 13.

B. A scheme of a Ps WGS experiment

Due to the same arguments as in the case of $\overline{\text{H}}$, the scheme of a Ps experiment is the same as the scheme of the $\overline{\text{H}}$ experiment. In this case, a PET-like detector would be used to reconstruct the annihilation vertex of Ps on the mirror.

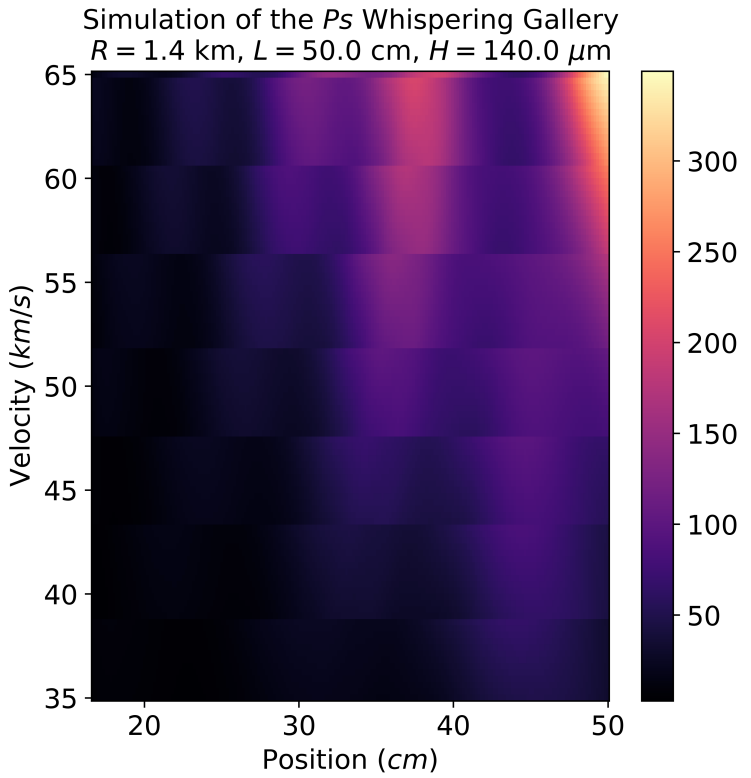

FIG. 13. A simulation of the annihilation rate of Ps on the surface of a mirror with the parameters in Eq. (91). Similar to the calculation of Mu, only the absorber/scatterer free region is shown. The absorber/scatterer has a length of $L_a = 16.6$ cm in this calculation.

C. A possible improvement

Although it seems feasible to measure the WGS of Ps and the QR can be studied, the detection of the gravitational shift is much more difficult. The results shown in the previous sections are on the border between "very challenging" and "impossible". However, unlike Mu, whose lifetime cannot be changed, the lifetime of Ps can be, in principle, increased using excited states with $n > 33$. This change may increase the relative magnitude of the gravitational shift (see Eq. 86), which is proportional to $(\tau^{\rm Ps})^{1.5}$ which is quite a strong factor. In this case, the gravitational shift could be measured as well. We should remember that the mirror size should then increase and/or the velocity decrease.

A particular difficulty that must be studied in detail is that the critical energy of all materials for Ps (and Mu) is "too" high. Therefore, the annihilation probability per quasi-classical bounce is very low, and the preferred material should have a minimal critical energy.

This difficulty is due to the fact that we wanted to optimize the sensitivity to gravitational shifts. If QR is the main goal, then the experiment is much simpler. We have to decrease the mirror radius to get WGS energies comparable to the effective critical energy of the mirror. In this case, the probability of annihilation (thus statistics) is high.

IX. CONCLUSION

We presented a general method for optimizing experiments that rely on gravitational and other shifts of the whispering-gallery interference patterns of different particles and atoms. A relatively small change in the key initial parameters of the problem leads to a change in the WGS parameters by many orders of magnitude, and thus simplifies the optimization of experiments for solving specific problems. This approach has been applied to particles and atoms such as neutrons, hydrogen, antihydrogen, muonium, and positronium. It can be extended to other particles, other experimental arrangements, and combinations of them. We proposed specific parameters and experimental schemes to observe the whispering-gallery interference patterns and their shifts. Note that each of the cases considered can be viewed as a "zero approximation" and a proof of the feasibility of the corresponding experiment. The sensitivity/accuracy of these experiments might be significantly increased by "fine-tuning" the parameters of the problem, increasing the (spatial, temporal, energetic, etc.) resolutions, increasing the statistics and properties of the particle beams, etc. The proposed method has numerous applications. In particular, the proposed neutron interferometer has high sensitivity and can be used to measure the gravitational constant and improve the constraint on the electric charge of the neutron. The hydrogen interferometer provides unprecedented sensitivity to the quantum reflection properties of hydrogen atoms from surfaces. All presented methods can be extended to heavier atoms. The antihydrogen interferometer can be implemented with antihydrogen velocities of at least $\sim 10^5$ m/s. The identification and use of materials with an effective critical energy greater than that of silica would further increase the upper limit of the antihydrogen velocity range. Even a velocity of $\sim 10^6$ m/s is possible only with the use of a complex and expensive cryogenic device. If the velocity is not significantly larger than $\sim 10^4$ m/s, measurements of a gravitational shift are experimentally feasible. Antihydrogen and positronium interferometers offer an advantage for studying quantum reflection in that antimatter particles are annihilated upon contact with

a surface, thus preventing spurious effects. Positronium interferometers can in principle allow one to measure gravitational shifts, although extremely challenging absolute precision is needed. Neutron, atom, and antiatom interferometers, under reduced gravity, provide long-lived quantum states and exhibit significantly increased sensitivity and precision.

ACKNOWLEDGMENTS

The authors thank all members of the GRASIAN, GRANIT, and GBAR collaborations for the fruitful and stimulating discussions. JP and SB are supported by the National Science Foundation under grant PHY-2412782.

---

[1] J. Strutt, *The Theory of Sound, Vol. 2, s. 1* (Macmillian, 1878).

[2] L. Rayleigh, The problem of the whispering gallery, Phil. Mag. **20**, 10001 (1910).

[3] L. Rayleigh, Further applications of bessel's functions of high order to the whispering gallery and allied problems, Phil. Mag. **27**, 100 (1914).

[4] C. Raman, On whispering galleries, Proc. Ind. Ass. Cult. Sci. **7**, 159 (1921-1922).

[5] G. Mie, Beiträge zur optik trüber medien, speziell kolloidaler metallösungen, Ann. Phys. **25**, 377 (1908).

[6] P. Debey, Der lichtdruck auf kugeln von beliebigem material, Ann. Phys. **30**, 57 (1909).

[7] K. Budden *et al.*, The ionosphere as a whispering gallery, Proc. Roy. Soc. Lond. **265**, 554 (1962).

[8] C. Liu *et al.*, Surface trapped x rays: whispering gallery modes at lambda = 0.7 a, Phys. Rev. Lett. **79**, 788 (1997).

[9] A. Oraevsky, Whispering-gallery waves, Quant. Electron. **32**, 377 (2002).

[10] K. Vahala, Optical microcavities, Nature **424**, 839 (2003).

[11] P. Stanwix *et al.*, Test of lorentz invariance in electrodynamics using rotating cryogenic sapphire microwave oscillators, Phys. Rev. Lett. **95**, 040404 (2005).

[12] I. Grudinin *et al.*, Ultrahigh optical q factor of crystalline resonators in the linear regime, Phys. Rev. A **76**, 063806 (2006).

[13] P. DelHaye *et al.*, Optical frequency comb generation from a monolithic microresonator, Nature **450**, 1214 (2007).

[14] T. Kippenberg *et al.*, Cavity optomechanics: back-action at the mesoscale, Science **321**, 1172 (2008).

[15] J. Hyun *et al.*, Measruring far-ultraviolet whispering gallery modes with high energy electrons, Appl. Phys. Lett. **93**, 243106 (2008).

[16] R. Mendis *et al.*, Whispering-gallery-mode terahertz pulse propagation on a curved metallic plate, Appl. Phys. Lett. **97**, 031106 (2010).

[17] A. Chiasera *et al.*, Spherical whispering-gallery-mode microresonators, Laser Photon. Rev. **4**, 457 (2010).

[18] F. Albert *et al.*, Whispering gallery mode lasing in electrically driven quantum dot micropillars, Appl. Phys. Lett. **97**, 101108 (2010).

[19] H. Mabuchi *et al.*, Atom galleries for whispering atoms - binding atoms in stable orbits around an optical resonator, Opt. Lett. **19**, 749 (1994).

[20] D. Vernooy *et al.*, Quantum structure and dynamics for atom galleries, Phys. Rev. A **SS**, 1239 (1997).

[21] A. Voronin *et al.*, Whispering gallery states of antihydrogen near a curved surface, Phys. Rev. A **85**, 014902 (2012).

[22] V. Nesvizhevsky *et al.*, Centrifugal quantum states of neutrons, Phys. Rev. A **78**, 033616 (2008).

[23] R. Cubitt *et al.*, Methods of observation of the centrifugal quantum states of neutrons, Nucl. Instr. Meth. A **611**, 322 (2009).

[24] V. Nesvizhevsky *et al.*, Neutron whispering gallery, Nature Phys. **6**, 114 (2010).

[25] V. Nesvizhevsky *et al.*, Centrifugal quantum states of neutrons, Compt. Rend. Phys. **12**, 791 (2011).

[26] G. Reecht *et al.*, Oligothiophene nanorings as electron resonators for whispering gallery modes, Phys. Rev. Lett. **110**, 056802 (2013).

[27] H. Rauch, Neutrons in a whispering gallery, Nature Phys. **6**, 79 (2010).

[28] E. Fermi, Sul moto dei neutroni nelle sostanze idrogenate, Ric. Sci. **7**, 13 (1936).

[29] K. Schreiner *et al.*, Measurement of magnetic shift of neutron whispering gallery, unpublished.

[30] G. Dufour *et al.*, Quantum reflection of antihydrogen from the casimir potential above matter slabs, Phys. Rev. A **87**, 012901 (2013).

[31] J. Lennard-Jones *et al.*, The interaction of atoms and molecules with solid surfaces. iii, Proc. R. Soc. London A **156**, 6 (1936).

[32] J. Lennard-Jones *et al.*, The interaction of atoms and molecules with solid surfaces. iv, Proc. R. Soc. London A **156**, 29 (1936).

[33] M. Berry *et al.*, Semiclassical approximation in wave mechanics, Rep. Prog. Phys. **35**, 315 (1972).

[34] I. Yu *et al.*, Evidence for universal quantum reflection of hydrogen from liquid he-4, Phys. Rev. Lett. **71**, 1589 (1993).

[35] J. Berkhout *et al.*, Scattering of hydrogen atoms from liquid-helium surfaces, Phys. Rev. B **47**, 8886 (1993).

[36] C. Carraro *et al.*, Sticking coefficient at ultralow energy: Quantum reflection, Prog. Surf. Sci. **57**, 61 (1998).

[37] F. Shimizu, Specular reflection of very slow metastable neon atoms from a solid surface, Phys. Rev. Lett. **86**, 987 (2001).

[38] V. Druzhinina *et al.*, Experimental observation of quantum reflection far from thrshold, Phys. Rev. Lett. **91**, 193202 (2003).

[39] T. Pasquini *et al.*, Quantum reflection from a solid surface at normal incidence, Phys. Rev. Lett. **93**, 223201 (2004).

[40] H. Friedrich *et al.*, Working with wkb waves far from the semiclassical limit, Phys. Rep. **397**, 359 (2004).

[41] H. Oberst *et al.*, Quantum reflection of he* on silicon, Phys. Rev. A **71**, 052901 (2005).

[42] T. Pasquini *et al.*, Low velocity quantum reflection of bose-einstein condensates, Phys. Rev. Lett. **97**, 093201 (2006).

[43] B. Zhao *et al.*, Quantum reflection of helium atom beams from a microstructured grating, Phys. Rev. A **78**, 010902 (2008).

[44] A. Voronin *et al.*, Quantum reflection of ultracold antihydrogen from a solid surface, J. Phys. B **38**, L301 (2005).

[45] P. Froelich *et al.*, Interation of antihydrogen with ordinary atoms and solid surfaces, Hyperf. Inter. **213**, 115 (2012).

[46] O. Bertolami *et al.*, Ultracold neutrons, quantum effects of gravity and the weak equivalence principle, Class. Quant. Grav. **20**, L61 (2003).

[47] O. Bertolami *et al.*, Noncommutative gravitational quantum well, Phys. Rev. D **72**, 025010 (2005).

[48] F. Blau *et al.*, Minimal length uncertainty relation and gravitational quantum well, Phys. Rev. D **74**, 036002 (2006).

[49] S. Baeßler *et al.*, Constraint on the coupling of axionlike particles to matter via an ultracold neutron gravitational experiment, Phys. Rev. D **75**, 075006 (2007).

[50] A. Saha, Time-space non-commutativity in gravitational quantum well scenario, Europ. Phys. J. C **51**, 199 (2007).

[51] C. Bastos, Berry phase in the gravitational quantum well and the seiberg-witten map, Phys. Lett. A **372**, 5556 (2008).

[52] S. Baeßler, Gravitationally bound quantum states of ultracold neutrons and their applications, J. Phys. G **36**, 104005 (2009).

[53] K. Nozari *et al.*, Minimal length and bouncing-particle spectrum, Europ. Phys. Lett. **92**, 50013 (2010).

[54] E. Kajari *et al.*, Inertial and gravitational mass in quantum mechanics, Appl. Phys. B **100**, 43 (2010).

[55] C. Bastos *et al.*, Entropic gravity, phase-space noncommutativity and the equivalence principle, Class. Quant. Grav. **28**, 125007 (2011).

[56] P. Pedram *et al.*, The effects of minimal length and maximal momentum on the transition rate of ultra cold neutrons in gravitational field, J. High En. Phys. **3**, 093 (2011).

[57] P. Brax *et al.*, Strongly coupled chameleons and the neutronic quantum bouncer, Phys. Rev. Lett. **107**, 111301 (2011).

[58] A. Kobakhidze, Gravity is not an entropic force, Europ. Phys. J. C **57**, 835 (2011).

[59] L. Chang *et al.*, On the minimal length uncertainty relation and the foundations of string theory, Adv. High En. Phys. **211**, 493514 (2011).

[60] E. Romera, Revivals of zitterbewegung of a bound localized dirac particle, Phys. Rev. A **84**, 052102 (2011).

[61] T. Jenke *et al.*, Realization of a gravity-resonance-spectroscopy technique, Nature Physics **7**, 468 (2011).

[62] P. Brax, Probing strongly coupled chameleons with slow neutrons, Phys. Rev. D **88**, 083004 (2013).

[63] E. Abreu *et al.*, Considerations on gravity as an entropic force and entangled states, Phys. Lett. B **727**, 524 (2013).

[64] M. Belloni *et al.*, The infinite well and dirac delta function potentials as pedagogical, mathematical and physical models in quantum mechanics, Phys. Rep. **540**, 25 (2014).

[65] T. Jenke *et al.*, Gravity resonance spectroscopy constrains dark energy and dark matter scenarios, Phys. Rev. Lett. **112**, 151105 (2014).

[66] G. Pignol, Probing dark energy models with neutrons, Int. J. Mod. Phys. A **30**, 1530048 (2015).

[67] N. Altamirano *et al.*, Gravity is not a pairwise local classical channel, Class. Quant. Grav. **35**, 145005 (2018).

[68] C. Anastopoulos *et al.*, Quantum superposition of two gravitational cat states, Class. Quant. Grav. **37**, 235012 (2020).

[69] T. Krisnanda *et al.*, Observable quantum entanglement due to gravity, NPJ Quant. Inf. **6**, 12 (2020).

[70] V. Nesvizhevsky *et al.*, Quantum states of neutrons in the earth's gravitational field, Nature **415**, 297 (2002).

[71] G. Dufour *et al.*, Shaping the distribution of vertical velocities of antihydrogen in gbar, Europ. Phys. J. C **74**, 2731 (2014).

[72] V. Nesvizhevsky *et al.*, Interference of several gravitational quantum states of antihydrogen in gbar experiment, Hyperf. Inter. **240**, 32 (2019).

[73] P. Crepin *et al.*, Quantum interference test of the equivalence principle on antihydrogen, Phys. Rev. A **99**, 042119 (2019).

[74] B. Dobrescu *et al.*, Spin-dependent macroscopic forces from new particle exchange, J. High En. Phys. **2006**, 005 (2006).

[75] I. Antoniadis *et al.*, Short-range fundamental forces, Compt. Rend. Phys. **12**, 755 (2011).

[76] M. Safronova *et al.*, Search for new physics with atoms and molecules, Rev. Mod. Phys. **90**, 025008 (2018).

[77] P. Fadeev *et al.*, Revisiting spin-dependent forces mediated by new bosons: Potentials in the coordinate-space representation for macroscopic- and atomic-scale experiments, Phys. Rev.

A **99**, 022113 (2019).

[78] J. Kimball *et al.*, Probing fundamental physics with spin-based quantum sensors, Phys. Rev. A **108**, 010101 (2023).

[79] V. Kostelecký *et al.*, Matter-gravity couplings and lorentz violation, Phys. Rev. D **83**, 016013 (2011).

[80] R. Colella *et al.*, Observation of gravitationally induced quantum interference, Phys. Rev. Lett. **34**, 1472 (1975).

[81] C. Killian *et al.*, Grasian: towards the first demonstration of gravitational quantum states of atoms with a cryogenic hydrogen beam, Europ. Phys. J. D **77**, 50 (2023).

[82] C. Killian *et al.*, Grasian: shaping and characterization of the cold hydrogen and deuterium beams for the forthcoming first demonstration of gravitational quantum states of atoms, Europ. Phys. J. D **78**, 132 (2024).

[83] A. Charman *et al.*, Description and first application of a new technique to measure the gravitational mass of antihydrogen, Nature Com. **4**, 1785 (2013).

[84] A. Kellerbauer *et al.*, Proposed antimatter gravity measurement with an antihydrogen beam, Nucl. Instr. Meth. B **266**, 351 (2008).

[85] P. Indelicato *et al.*, The gbar project, or how does antimatter fall?, Hyperf. Inter. **228**, 141 (2014).

[86] P. Perez *et al.*, The gbar antimatter gravity experiment, Hyperf. Inter. **233**, 21 (2015).

[87] W. Bertsche, Prospects for comparison of matter and antimatter gravitation with alpha-g, Phil. Trans. R. Soc. **376**, 0265 (2018).

[88] E. Anderson *et al.*, Observation of the effect of gravity on the motion of antimatter, Nature **621**, 716 (2023).

[89] E. D. Hunter *et al.*, Measured properties of an antihydrogen beam (2025), arXiv:2509.02583 [physics.ins-det].

[90] J. Zhang, *Development of a Novel Cryogenic Muonium Beam for the Measurement of the Gravitational Acceleration of Muonium*, Ph.D. thesis, Zurich, ETH (2025).

[91] V. Lushchikov *et al.*, Observation of ultracold neutrons, JETP Lett. **9**, 23 (1969).

[92] V. V. Nesvizhevsky *et al.*, The whispering gallery effect in neutron scattering, New J. Phys. **12**, 113050 (2010).

[93] V. V. Nesvizhevsky *et al.*, Search for quantum states of the neutron in a gravitational field:: gravitational levels, Nucl. Instrum. Meth. A **440**, 754 (2000).

[94] V. V. Nesvizhevsky *et al.*, Study of the neutron quantum states in the gravity field, Europ. Phys. J. C **40**, 479 (2005).

[95] A. Y. Voronin *et al.*, Quantum motion of a neutron in a waveguide in the gravitational field, Phys. Rev. D **73**, 044029 (2006).

[96] A. E. Meyerovich *et al.*, Gravitational quantum states of neutrons in a rough waveguide, Phys. Rev. A **73**, 063616 (2006).

[97] R. Adhikari *et al.*, Quantum size effect and biased diffusion of gravitationally bound neutrons in a rough waveguide, Phys. Rev. A **75**, 063613 (2007).

[98] V. Nesvizhevsky, Near-surface quantum states of neutrons in the gravitational and centrifugal potentials, Physics-Uspechi **53**, 645 (2010).

[99] M. Escobar *et al.*, Rough mirror as a quantum state selector: Analysis and design, Adv. High En. Phys. **2014**, 764182 (2014).

[100] D. C. Brody, Biorthogonal quantum mechanics, Journal of Physics A: Mathematical and Theoretical **47**, 035305 (2014).

[101] G. Dufour, *Quantum reflection from the Casimir-Polder potential*, Thèse de doctorat, Université Pierre et Marie Curie (Sorbonne Universités), Paris, France (2015), thèse réalisée au Laboratoire Kastler-Brossel, École doctorale Physique en Île-de-France.

[102] S. Schlamminger *et al.*, Test of the equivalence principle using a rotating torsion balance, Phys. Rev. Lett. **100**, 041101 (2008).

[103] P. Touboul *et al.* (MICROSCOPE Collaboration), *microscope* mission: Final results of the test of the equivalence principle, Phys. Rev. Lett. **129**, 121102 (2022).

[104] V. V. Nesvizhevsky *et al.*, Measurement of quantum states of neutrons in the earth's gravitational field, Phys. Rev. D **67**, 102002 (2003).

[105] J. Jakubek *et al.*, A coated pixel device timepix with micron spatial resolution for ucn detection, Nucl. Instr. Meth. A **600**, 651 (2009).

[106] J. Jakubek *et al.*, Position-sensitive spectroscopy of ultra-cold neutrons with timepix pixel detector, Nucl. Instr. Meth. A **607**, 45 (2009).

[107] S. Kawasaki *et al.*, Development of a pixel detector for ultracold neutrons, Nucl. Instr. Meth. A **615**, 42 (2010).

[108] S. Kamiya *et al.*, Development of a neutron imaging sensor using intpix4-soi pixelated silicon devices, Nucl. Instr. Meth. A **979**, 164400 (2020).

[109] B. Clement *et al.*, Spatial resolution determination of a position sensitive ultra-cold neutron detector, Nucl. Instr. Meth. A **1040**, 167212 (2022).

[110] G. Pignol *et al.*, Granit project: a trap for gravitational quantum states of ucn (2007), arXiv:0708.2541 [quant-ph].

[111] A. Westphal *et al.*, A quantum mechanical description of the experiment on the observation of gravitationally bound states, Europ. Phys. J. C **51**, 367 (2007).

[112] Y. V. Borisov *et al.*, Study of potential application of ultracold neutrons for measuring the neutron electric charge, Zhurn. Techn. Phys. **58**, 951 (1988).

[113] V. V. Nesvizhevsky, Polished sapphire for ultracold-neutron guides, Nucl. Instrum. Meth. A **557**, 576 (2006).

[114] V. V. Nesvizhevsky *et al.*, Comparison of specularly reflecting mirrors for granit, Nucl. Instrum. Meth. A **578**, 435 (2007).

[115] CODATA, 2022 codata value: Newtonian constant of gravitation. the nist reference on constants, units, and uncertainty, (2024).

[116] J. Baumann *et al.*, Experimental limit for the charge of the free neutron, Phys. Rev. D **37**, 3107 (1988).

[117] G. Dufour *et al.*, Quantum reflection of antihydrogen from nanoporous media, Phys. Rev. A **87**, 022506 (2013).

[118] P. Crepin *et al.*, Quantum reflection of antihydrogen from a liquid helium film, Europ. Phys. Lett. **119**, 33001 (2017).

[119] P. Crepin *et al.*, Quantum reflection of antihydrogen from a liquid helium bulk, Hyperf. Inter. **240**, 58 (2019).

[120] S. Cooper *et al.*, Cryogenic atomic hydrogen beam apparatus with velocity characterization, Rev. Sci. Inst. **91**, 013201 (2020).

[121] J. Ahokas *et al.*, A large octupole magnetic trap for research with atomic hydrogen, Rev. Sci. Instr. **93**, 023201 (2022).

[122] A. Semakin *et al.*, Cold source of atomic hydrogen for loading large magnetic traps, Europ. Phys. J. D **79**, 23 (2025).

[123] P. Adrich *et al.*, Production of antihydrogen atoms by 6 kev antiprotons through a positronium cloud, Europ. Phys. J. C **83**, 1004 (2023).

[124] V. V. Nesvizhevsky *et al.*, A magneto-gravitational trap for studies of gravitational quantum states, Europ. Phys. J. C **80**, 520 (2020).

[125] A. Antognini *et al.*, Muonium emission into vacuum from mesoporous thin films at cryogenic temperatures, Phys. Rev. Lett. **108**, 143401 (2012), arXiv:1112.4887 [physics.atom-ph].

[126] D. Maso *et al.*, Future facilities at PSI, the high-intensity muon beams (HIMB) project, in *Europ. Phys. J. Web Conf.*, Vol. 282 (EDP Sciences, 2023) p. 01012.

[127] M. Saarela and E. Krotscheck, Hydrogen isotope and [sup 3]he impurities in liquid [sup 4]he, J. Low Temp. Phys. **90**, 10.1007/BF00681890 (1993).

[128] A. Soter *et al.*, Development of a cold atomic muonium beam for next generation atomic physics and gravity experiments, SciPost Phys. Proc. , 031 (2021).

[129] A. Abele *et al.*, Characterization of a ballistic supermirror neutron guide, Europ. Phys. J. D **562**, 407 (2006).

[130] P. Crivelli *et al.*, Measurement of the orthopositronium confinement energy in mesoporous thin films, Phys. Rev. A **81**, 052703 (2010).

[131] D. Cassidy *et al.*, Positronium cooling in porous silica measured via doppler spectroscopy, Phys. Rev. A **81**, 012715 (2010).

[132] J. Guyomard *et al.*, Single-bounce quantum gravimeter to measure the free-fall of antihydrogen, arXiv preprint arXiv:2505.04771 (2025), preprint; posted 9 May 2025.

Appendix A: Stationary Phase Approximation

The stationary phase approximation is used to approximate Eq. (21) as Eq. (22). The details of the approximation are worked out here. We can rewrite Eq. (21) as

$$\Psi(x,z) \approx \frac{1}{\sqrt{2\pi}} e^{ik_0 z} \int_{-\infty}^{\infty} \tilde{\psi}(k) e^{i\phi(k)} dk \quad , \tag{A1}$$

where

$$\phi(k) = -\frac{k^2}{2k_0} z + kx \quad . \tag{A2}$$

The phase rapidly oscillates for k of the relevant scale describing the wave packet, so much of this integral cancels beyond the stationary point of $\phi(k)$. The stationary point of of Eq.

(A2) occurs for $k = k_s$ with

$$k_s = k_0 \frac{x}{z} \quad . \tag{A3}$$

Note also that

$$\frac{\partial^2 \phi}{\partial k^2}(k_s) = -\frac{z}{k_0} \quad . \tag{A4}$$

Using Eqs. (A2 - A4), the phase can be approximated about its stationary point as

$$\begin{aligned} \phi(k) \approx & \phi(k_s) + \frac{1}{2}\frac{\partial^2 \phi}{\partial k^2}(k_s)(k-k_s)^2 \\ = & \frac{k_0}{z}\frac{x^2}{2} - \frac{z}{2k_0}\left(k - k_0\frac{x}{z}\right)^2 \quad . \end{aligned} \tag{A5}$$

If we approximate $\tilde{\psi}$ to zeroth order of k_s, we find the approximate position space wave function to be

$$\Psi(x,z) \approx \frac{1}{\sqrt{2\pi}} \tilde{\psi}\left(k_0\frac{x}{z}\right) e^{i\left(k_0 z + \frac{k_0}{z}\frac{x^2}{2}\right)} \int_{-\infty}^{\infty} e^{-i\frac{z}{2k_0}\left(k - k_0\frac{x}{z}\right)^2} dk \quad . \tag{A6}$$

By changing the coordinates from $k \to s$ where $s = \sqrt{\frac{z}{2k_0}}\left(k - k_0\frac{x}{z}\right)$ we find the above integral becomes

$$\Psi(x,z) \approx \tilde{\psi}\left(k_0\frac{x}{z}\right) e^{i\left(k_0 z + \frac{k_0}{z}\frac{x^2}{2}\right)} \sqrt{\frac{k_0}{\pi z}} \int_{-\infty}^{\infty} e^{-is^2} ds \quad . \tag{A7}$$

The above expression is the Fresnel integral and has the value

$$\int_{-\infty}^{\infty} e^{-is^2} ds = \sqrt{\pi} e^{i\frac{\pi}{4}} \quad . \tag{A8}$$

and we find that

$$\Psi(x,z) \approx \sqrt{\frac{k_0}{z}} \tilde{\psi}\left(k_0\frac{x}{z}\right) e^{i\left(k_0 z + \frac{k_0}{z}\frac{x^2}{2} + \frac{\pi}{4}\right)} \quad . \tag{A9}$$

Appendix B: Sensitivity Estimate

To estimate the sensitivity of the described experiments to an external force, we calculate the Cramér-Rao bound on the variance $\sigma_{\hat{a}}^2$ of the estimator $\hat{a}$ of the applied acceleration a. This method has been used to estimate the sensitivity of similar experiments in [73, 132]. This estimation will assume $\hat{a}$ is unbiased and efficient, an assumption that should be tested directly with Monte-Carlo simulations. This bound can be calculated as the inverse of the Fisher information

$$\mathcal{I} = \mathbb{E}\left[\left(\frac{\partial \log \mathcal{L}}{\partial a}\right)^2\right] \quad , \tag{B1}$$

where $\mathcal{L}$ is the likelihood function for an experiment that samples the probability distribution $P(X, V, a, \vec{\theta})$ N times. P corresponds to the simulated interference patterns, X is the position, V the velocity, and $\vec{\theta}$ are nuisance parameters. With the likelihood defined as

$$\mathcal{L} = \prod_{i=1}^{N} P\left(X_i, V_i, a, \vec{\theta}\right) \quad , \tag{B2}$$

the Fisher information becomes

$$\begin{aligned} \mathcal{I} &= \int \cdots \int \sum_{i=1}^{N} \left(\frac{\partial}{\partial a} \log P(X_i, V_i, a, \vec{\theta}) \right)^2 \prod_{j=1}^{N} P(X_j, V_j, a, \vec{\theta}) dX_j dV_j \\ &= N \int \int \frac{\left(\frac{\partial}{\partial a} P(X, V, a, \vec{\theta}) \right)^2}{P(X, V, a, \vec{\theta})} dX dV \quad , \end{aligned} \tag{B3}$$

where X_i, V_i are the coordinates of the sampled event. The Cramér-Rao bound estimate on the error $\hat{a}$ is then

$$\sigma_{\hat{a}} = \frac{1}{\sqrt{N}} \left(\int \int \frac{\left(\frac{\partial}{\partial a} P(X, V, a, \vec{\theta}) \right)^2}{P(X, V, a, \vec{\theta})} dX dV \right)^{-\frac{1}{2}} \quad . \tag{B4}$$